



Author: Jiahui Li, Yvonne Durandet, Xiaodong Huang, Guangyong Sun, Dong Ruan
Title: Additively manufactured fiber-reinforced composites: A review of mechanical behavior and opportunities
Year: 2022
Journal: Journal of Materials Science & Technology
Volume: 119
Pages: 219-244
URL: <http://hdl.handle.net/1959.3/466417>

Copyright: Copyright © 2022 the authors.

This is the author's final peer-reviewed accepted manuscript version, hosted under the terms and conditions of the Attribution-NonCommercial 4.0 International (CC BY-NC 4.0) license.
See <http://creativecommons.org/licenses/by-nc/4.0/>

The published version is available at: <https://doi.org/10.1016/j.jmst.2021.11.063>

Additively manufactured fiber-reinforced composites: a review of mechanical behavior and opportunities

Jiahui Li ^a, Yvonne Durandet ^a, Xiaodong Huang ^a, Guangyong Sun ^b, Dong Ruan ^{a,*}

^a Department of Mechanical Engineering and Product Design Engineering, School of Engineering, Swinburne University of Technology, Hawthorn, VIC 3122, Australia

^b State Key Laboratory of Advanced Design and Manufacture for Vehicle Body, Hunan University, Changsha 410082, China

*Corresponding Author.

Email: druan@swin.edu.au (D. Ruan).

Abstract: Recent developments in additive manufacturing techniques have facilitated the fabrication of fiber-reinforced composite materials. In this paper, the mechanical properties and deformation mechanisms of discontinuous and continuous fiber-reinforced composites fabricated by various additive manufacturing techniques are comprehensively reviewed. The effects of fiber type, orientation and weight/volume fraction, printing path, and stacking sequence on the mechanical properties of additively manufactured composites are discussed. In addition, the applications of additively manufactured composites, the main challenges of the current additive manufacturing techniques, and recommendations for future work are also presented.

Keywords: Additive manufacturing; Discontinuous and continuous fiber-reinforced composites; Mechanical properties; Deformation mechanism; Applications

Table of Contents

1.	Introduction	3
2.	Discontinuous FRCs: AM techniques and resulting mechanical properties	5
2.1.	FDM and the mechanical properties of FDM-fabricated discontinuous FRCs	6
2.1.1	Fused Deposition Modeling (FDM)	6
2.1.2	Mechanical properties of FDM-fabricated discontinuous FRCs	7
2.2.	DIW and the mechanical properties of DIW-fabricated discontinuous FRCs	14
2.2.1	Direct Ink Writing (DIW)	14
2.2.2	Mechanical properties of DIW-fabricated discontinuous FRCs	15
2.3.	SLS and the mechanical properties of SLS-fabricated discontinuous FRCs	16
2.3.1	Selective Laser Sintering (SLS)	16
2.3.2	Mechanical properties of SLS-fabricated discontinuous FRCs	17
2.4.	SLA and the mechanical properties of SLA-fabricated discontinuous FRCs	19
2.4.1	Stereolithography (SLA)	19
2.4.2	Mechanical properties of SLA-fabricated discontinuous FRCs	20
2.5.	Comparison of the mechanical properties of discontinuous FRCs fabricated using FDM, DIW, SLS and SLA	21
3.	Continuous FRCs: AM techniques and resulting mechanical properties	23
3.1.	FDM and the mechanical properties of FDM-fabricated continuous FRCs	24
3.1.1	Fused Deposition Modeling (FDM)	24
3.1.2	Mechanical properties of FDM-fabricated continuous FRCs	25
3.2.	SLA and mechanical properties of SLA-fabricated continuous FRCs	34
3.3.	Mechanical properties of LOM-fabricated continuous FRCs	35
3.4.	Comparison of the tensile properties of continuous FRCs manufactured via different AM techniques	37
4.	Applications of AM-fabricated fiber reinforced composites	40
4.1.	Tools and molds	40
4.2.	End-use products	41
5.	Limitations and recommendations for future work	43
5.1.	Feedstock materials for AM-fabricated FRCs	43
5.1.1	Fibers	43
5.1.2	Matrix	43
5.2.1	Printing logic	45
5.2.2	Slicing software	46
5.3.	Printing quality	47
5.4.	Mechanical properties of AM-fabricated FRCs	48
5.5.	Numerical simulation and theoretical prediction	49
6.	Summary	49

1. Introduction

High-performance fiber-reinforced composites (FRCs) offer high strength to weight ratio, low coefficient of thermal expansion, good resistance to corrosion, and high thermal conductivity. They have been widely used and play a pivotal role in ensuring continuous robust developments of a wide variety of industry sectors that are essential for our economy, including aerospace, aircraft, defense, construction, automotive, sport and energy industries. For example, each Boeing 787 Dreamliner aircraft has approximately 80% composites by volume with 32 tons of carbon fiber-reinforced composites. Thales Australia, an Australian armor vehicle manufacturer, uses a large number of composites in its landmark Hawke Protected Vehicle.

There are several traditional approaches to fabricate composite materials and structural components. However, most of them involve manual layup of the layers of a composite or the use of expensive curing equipment and tooling. These make the fabrication of FRCs using traditional methods labor and resource intensive. Recently developed additive manufacturing (AM) or 3D printing provides a convenient tool-less alternative to directly fabricate a small volume of newly designed, delicate spare parts, which would be costly and time-consuming to produce using traditional manufacturing methods such as molding. Moreover, the geometry of a part can be easily modified by AM to obtain an optimal structure that possesses the desired mechanical properties with minimum weight. These are the two key factors driving the growth of additive manufacturing of FRCs [1].

Fiber-reinforced composites can be categorized in two groups: discontinuous and continuous fiber-reinforced composites. Discontinuous fiber-reinforced composites have been fabricated using four AM techniques, namely Fused Deposition Modeling (FDM) using thermoplastic filaments, Direct Ink Writing (DIW) using thermoset epoxy resin, Selective Laser Sintering (SLS) using plastic powder, and Stereolithography apparatus (SLA) using photopolymer resin. Continuous fiber-reinforced composites have been manufactured via three

AM techniques, namely FDM, SLA, and LOM (Laminated Object Manufacturing) which uses plastic sheets. The most popular reinforced fibers employed with all AM techniques are carbon fiber (CF), glass fiber (GF) and Kevlar fiber (KF). Fibers are used in a form of either filaments or sheets. The most commonly used matrix materials are Nylon (e.g., PA6 and PA12), polylactic acid (PLA), and Acrylonitrile butadiene styrene (ABS). With recent developments in AM techniques, several types of printers are available to employ advanced matrix materials, such as polyether ether ketone (PEEK), which have better mechanical performance than Nylon, PLA and ABS [2].

Several review papers were published on the AM techniques to fabricate fiber-reinforced composites [3-8]. In 2017, Parandoush and Lin [3] discussed the manufacturing processes of all five AM techniques (FDM, DIW, SLS, SLA and LOM). Finite element method (FEM) and theoretical models, such as the modified rule of mixtures (MROM) and classical laminate plate theory (CLPT), to predict the mechanical properties of FRCs were appraised. Mechanical properties of AM-fabricated composites were presented with limited data available at that time. van de Werken et al. [4] focused on the state-of-the-art and perspective of AM-fabricated carbon fiber-reinforced composites only. Three review papers [5-7] dealt specifically with FDM. Brenken et al. [5] considered the physical phenomenon of FDM extrusion process and summarized tensile properties of FDM-fabricated FRCs. Kabir et al. [6] provided a summary of the development of FDM technique and mechanical properties of continuous fiber-reinforced composites only. The defects of FDM-fabricated FRCs and treatment methods to overcome these defects before and after printing were reviewed by Sachini et al. [7]. Le Duigou et al. [8] discussed AM-fabricated natural fiber-reinforced bio-composites and found that in most cases, the tensile moduli of discontinuous natural fiber-reinforced composites were slightly improved, while the tensile strengths were reduced [9,10].

To the best knowledge of the authors, no comprehensive review of the mechanical properties of AM-fabricated discontinuous and continuous fiber-reinforced composites using various AM techniques and diverse types of fibers is available yet. This paper reviews all five currently available AM techniques for fiber-reinforced composites (FDM, DIW, SLS, SLA and LOM), the mechanical properties (including tensile, flexural, compressive, shear, impact and fatigue properties) and the applications of AM-fabricated FRCs. In addition, limitations and suggestions for future work are also discussed.

2. Discontinuous FRCs: AM techniques and resulting mechanical properties

Various discontinuous synthetic and natural fibers were used as additions to enhance the mechanical properties of AM-fabricated FRCs [11-14]. Popular synthetic fibers include CF, GF and KF. The most commonly used discontinuous natural fibers are coconut fibers [9], wood fibers [10], jute fibers [15], and hemp fibers [16]. Since using natural fibers as reinforcement is not the focus of the current paper so the related mechanical data are not included.

Discontinuous fibers employed in AM fall into three categories according to their length or diameter: (1) nanofibers [17-19] with diameters much less than one micrometer, such as graphene nanoplates (x GnP), carbon nanofibers (CNFs), multi-walled carbon nanotubes (MWCNTs), carbon black and SiO₂ nanoparticles; (2) micro-fibers within the range of 50 μ m to 400 μ m in length [20, 21]; (3) milli-fibers with lengths at a millimeter scale. The fibers used in each of the four AM techniques to fabricate discontinuous FRCs are summarized in Table 1. It should be noted that milli-fibers can only be successfully used in SLA process. Although millimeter-long fibers can be used in FDM process, many fibers may break during the high shear melting and mixing process, and fibers are eventually shortened to approximately 400 μ m [21].

Table 1 Different types of reinforcing fibers used in various AM techniques

Fibers type	FDM	DIW	SLS	SLA
Nanofibers: diameter much less than 1 μm				
xGnPs	✓	✓	—	—
CNFs	✓	✓	✓	✓
MWCNTs	✓	✓	✓	✓
Carbon black	—	—	✓	✓
SiO ₂ nanoparticles	—	—	—	✓
Micro-fibers: diameter larger than 1 μm and length within 50 to 400 μm				
CF, GF and KF	✓	✓	✓	✓
SiC whiskers	—	✓	✓	—
Natural fibers	✓	—	—	—
Milli-fibers: longer than 400 μm				
CF and GF	—	—	—	✓

The four AM techniques (FDM, DIW, SLS and SLA) used to fabricate discontinuous FRCs, are each reviewed in the following subsections. The mechanical properties of discontinuous FRCs fabricated by these AM techniques are also discussed in these subsections.

2.1. FDM and the mechanical properties of FDM-fabricated discontinuous FRCs

2.1.1 Fused Deposition Modeling (FDM)

Although FDM techniques is not the first invented AM techniques, it is the most mature and developed techniques due to its simplicity and cost-effectiveness [22, 23]. Fig. 1(a) illustrates a typical FDM process [4]. The filament from the support material spool is firstly melted and deposited onto the build platform for several layers to form a foundation. The filament from the build material spool is made of discontinuous fibers and matrix and is subsequently deposited on top of this foundation. After one layer of build material is printed, the build platform moves one layer thickness down in the vertical direction to allow the fabrication of the next layer of build material. On completion of the fabrication process, the printed part is removed from the build platform and the support material is detached or dissolved using solvent [24]. Fig. 1(b) shows a sketch of a cross-sectional view of deposited

filaments in FDM [14]. The molten matrix material has a certain fluidity after extrusion, so it spreads and merges with the adjacent extruded filaments. Voids are normally observed between the printed filaments (Fig. 1(b)).

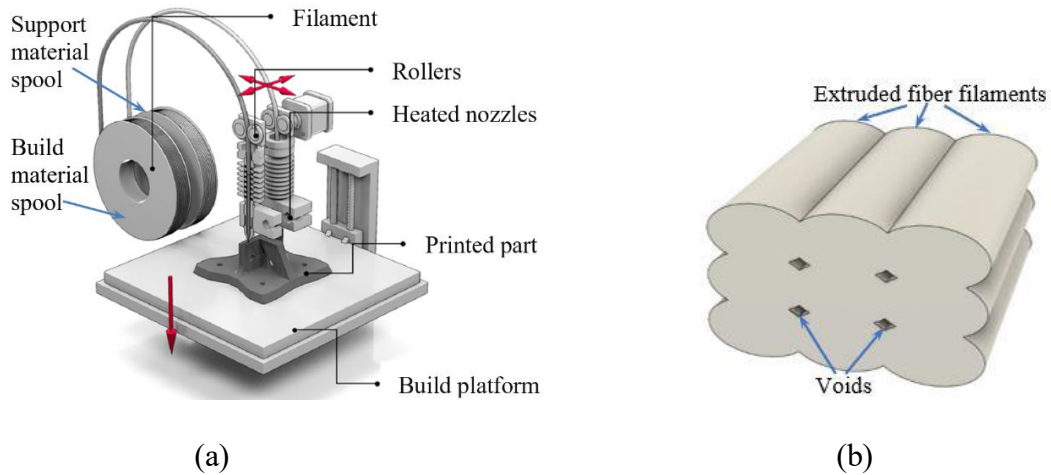


Fig. 1. Schematic of (a) a typical FDM process [4]; (b) cross-sectional view of deposited fiber filaments.

2.1.2 Mechanical properties of FDM-fabricated discontinuous FRCs

The mechanical properties of discontinuous FRCs vary with the fiber type [25, 26] and treatment of filaments [27], fiber weight percentage (wt.%) [28-31], fiber length [32], matrix [28, 29, 32-34], loading direction [25, 35, 36], and printing temperature [37, 38]. Several 3D printer suppliers, including Markforged, Stratasys, and 3DX, provide impregnated filaments with different types of fibers (e.g., CFs filled PA, PLA, ABS and PEEK filaments).

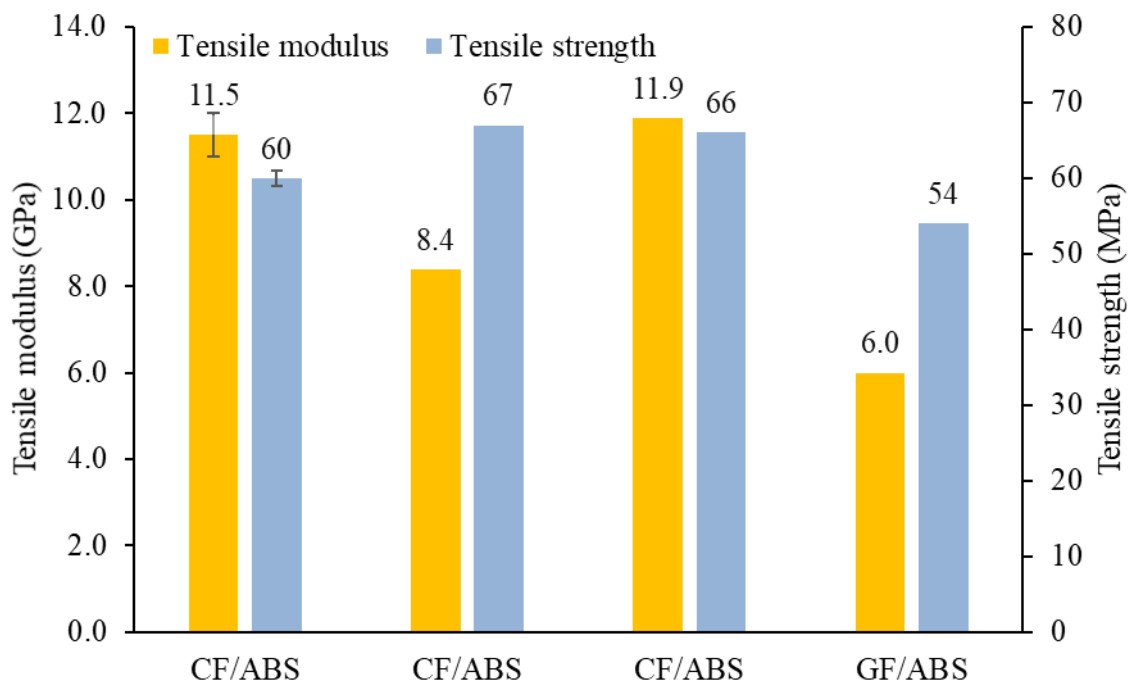
2.1.2.1 The effects of fiber type and treatment of filaments

Fiber types significantly affect the mechanical properties of AM-fabricated FRCs. For FDM fabricated discontinuous FRCs, CF and GF are the two most popular reinforcements, and their sizes are usually at a micro level. The reported mechanical properties of a single fiber strand are listed in Table 2.

Table 2 Mechanical properties of carbon and glass fibers (data from [39])

Fiber type	Young's modulus (GPa)	Tensile strength (MPa)	Specific strength (kN m/kg)
Carbon fiber	120 - 180	1600 - 4127	2457 - 3919
Glass fiber	30 - 40	1500 - 3450	1307 - 3300

In general, carbon FRCs are stronger than glass FRCs when using the same matrix material. Duty et al. [25] found the tensile modulus and strength of FDM-fabricated 20 wt.% CF/ABS were 11.9 GPa and 66 MPa respectively, while the tensile modulus and strength of 20 wt.% GF/ABS fabricated material were 5.7 GPa and 54 MPa respectively (Fig. (2)). Tekinalp et al. [26] also reported very similar tensile modulus (11.5 GPa) and strength (60 MPa) for 20 wt.% CF/ABS. Hill et al. [40] used the same fiber/matrix combination (20% CF/ABS) and achieved 8.4 GPa in tensile modulus and 67 MPa in tensile strength. On the other hand, when PEEK was used as the matrix, no significant discrepancies in both tensile and flexural properties were observed between CF/PEEK and GF/PEEK when the fiber weight percentages were the same [31].

**Fig. 2.** Tensile properties of FDM-fabricated 20 wt.% CF/ABS and GF/ABS FRCs (data from [25, 26, 40]).

The mechanical properties of FDM-fabricated discontinuous FRCs could be enhanced when filaments were pre-processed, i.e., by adding a consolidation step when preparing the reinforced filaments to achieve better processability to further increase the strength of final FRCs [29]. Yu et al. [34] modified the standard FDM process by adding a consolidation step, High Performance Discontinuous Fiber method (HPDF), when mixing and extruding the reinforced filaments. The tensile strength of a 12 wt.% CF/PA6 manufactured with consolidated filament at 200 °C was 250 MPa, which was approximately double that (84 MPa) of standard FDM-fabricated CF/PA6 with 17 wt.% fibers [29].

2.1.2.2 The effect of fiber weight percentage

The mechanical performance of some FDM-fabricated FRCs increases with fiber weight percentage when PA or PLA or ABS is the matrix, as the fibers have better mechanical properties than the matrix. Liao et al. [30] characterized the tensile modulus and strength of composites with various fiber weight percentages from zero to 10 wt.%. The tensile modulus of 10 wt.% CF/PA12 was 2.6 times higher than that of the pure PA12 matrix material (Fig. 3). Moreover, the tensile strength of CF/PA12 increased from 46 MPa to 94 MPa when the fiber weight percentage increased from zero and 10 wt.% (Fig. 3). Furthermore, Blok et al. [29], Tekinalp et al. [26] and Duty et al. [25] also found that tensile modulus and strength increased with fiber weight percentage for CF/PA6, CF/ABS and GF/ABS.

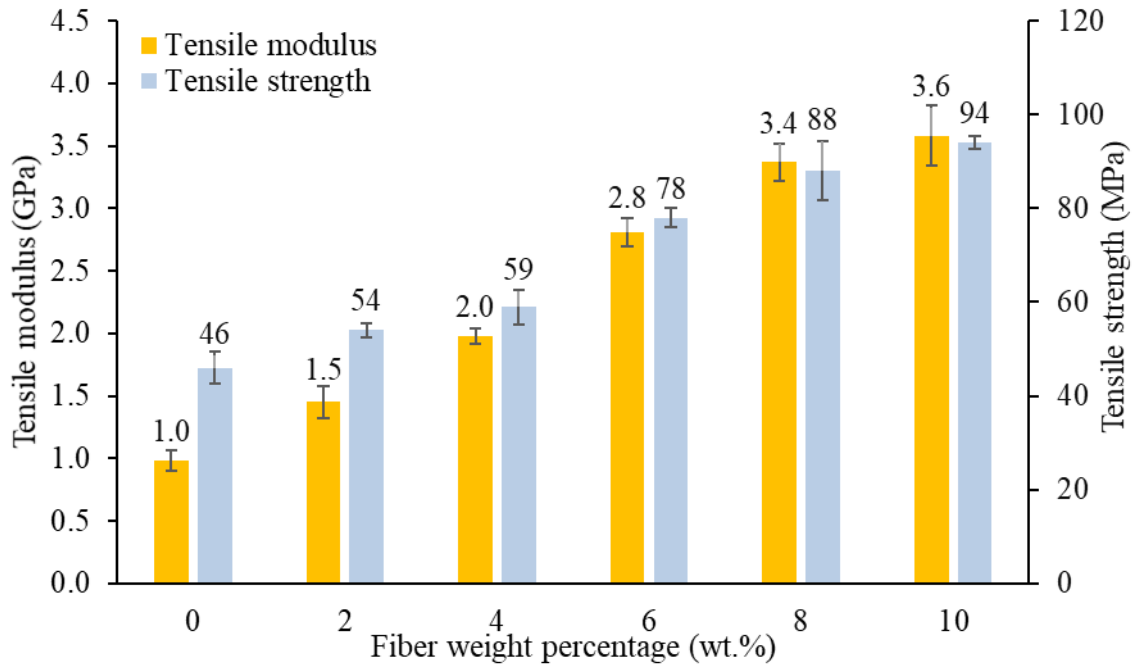


Fig. 3. Effect of fiber weight percentage on the tensile properties of FDM-fabricated CF/PA12 (data from [30]).

However, some researchers observed that mechanical properties of FDM-fabricated FRCs were not always improved with the increase of fiber weight percentage. Ning et al. [32] mixed ABS with carbon fibers of 0 wt.%, wt.%3, 5 wt.%, 7.5 wt.%, 10 wt.% and 15 wt.%. The tensile strength of CF/ABS increased to 43 MPa with fiber weight percentage from zero to 5 wt.%, then decreased to 34 MPa at 10 wt.%, and increased again to 36 MPa at 15 wt.%. Berretta et al. [28] tested the tensile strength of CNTs/PEEK with 0 wt.%, 1 wt.% and 5 wt.% CNTs and found that the tensile strength was improved to 70 MPa at 1 wt.% CNTs, while it decreased to 55 MPa at 5 wt.% CNTs. Both research groups attributed this unusual trend to the bonding between fibers and matrix.

On the other hand, both the tensile and flexural strengths of CF/PEEK and GF/PEEK decreased monotonically with the increase of fiber weight percentage in the range of 5 wt.% to 15 wt.% [31] (Fig. 4). Wang et al. [31] reported two reasons for this phenomenon: porosity and bonding between fibers and matrix. Firstly, as shown in Fig. 5(a1) – (c1), less pores appeared among the deposited paths at 5 wt.%; while more pores were observed inside not only within

printed beads, but also between layers when the fiber weight percentage was 15%. The amount and size of pores between printed beads increased with the weight percentage of fibers. Cracks might initiate from those pores and reduce the mechanical properties of FRCs. Secondly, pullout of many fibers was observed at 15 wt.% (Fig. 5(c2)), which stemmed from poor adhesion between fiber and matrix and resulted in low mechanical properties. Comparing Fig. 5(a2) with Fig. 5(b2), it is evident that the former has matrix residue on the fiber while the fiber surface of the latter is smooth without matrix residue.

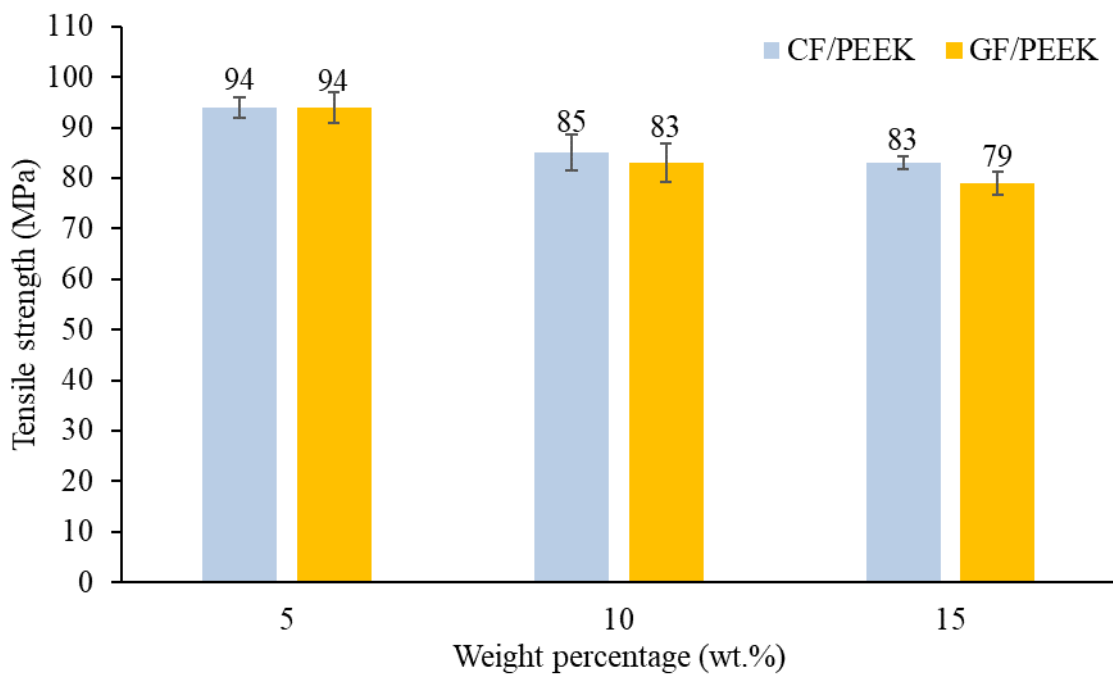


Fig. 4. Effect of fiber weight percentage on the tensile strength of FDM-fabricated CF/PEEK and GF/PEEK (data from [31]).

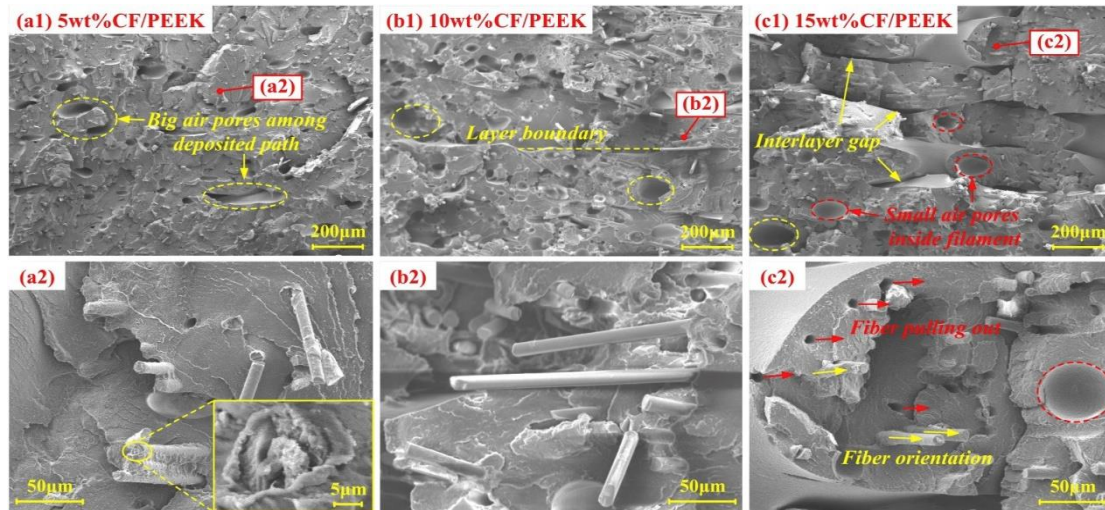


Fig. 5. SEM images of the fracture surfaces of AM-fabricated CF/PEEK with varied fiber weight percentage (a1) fracture surface of 5 wt.% CF/PEEK; (a2) enlargement of the area with pores; (b1) fracture surface of 10 wt.% CF/PEEK; (b2) enlargement of layer boundary; (c1) fracture surface of 15 wt.% CF/PEEK showing interlayer gaps; (c2) enlargement of pores inside filament [31].

2.1.2.3 The effect of fiber length

Ning et al. [32] compared the tensile properties of two types of specimens with the same fiber weight percentage (5 wt.%) but different fiber lengths (100 μm and 150 μm). The results showed that specimens with 150 μm carbon fiber length had larger Young's modulus (2.4 GPa) and tensile strength (45 MPa) than those with 100 μm carbon fiber length. However, due to the very limited studies on the effect of fiber length on mechanical properties of FDM-fabricated FRCs, no solid conclusion can be drawn yet.

2.1.2.4 The effect of matrix

PA (e.g., PA6 and PA12), PLA and ABS are three widely used matrix materials in FDM. Recently, new polymers such as PEEK have also been employed in FDM. Composites with PEEK as matrix have higher tensile strength than the composites using PLA or ABS as matrix due to the greater tensile strength of PEEK, while the tensile modulus of CF/PEEK composite is the smallest, but the reason is unknown. For example, the tensile modulus and strength of 15

wt.% carbon fiber-reinforced PLA, ABS and PEEK are 7.5 GPa and 53 MPa [36]; 8.9 GPa and 71 MPa [41]; 4.0 GPa and 83 MPa [31], respectively.

2.1.2.5 The effect of loading direction

Ferreira et al. [36] studied the tensile properties of CF/PLA by applying loads parallel and perpendicular to the printing directions. The tensile yield strength of CF/PLA loaded perpendicularly to the printing direction was only two-thirds of that of CF/PLA loaded along the printing direction. Duty et al. [25] conducted similar experiments on CF/ABS and found a dramatic drop of tensile strength from 66 MPa to 10 MPa under loadings along the printing direction and transverse direction, respectively. Love et al. [41] also reported a reduction in both tensile modulus and strength from 8.9 GPa and 71 MPa to 1.5 GPa and 7 MPa when the loading direction changed from longitudinal to transverse.

2.1.2.6 The effect of printing temperature

Printing temperature also plays an important role in the mechanical properties of printed materials as shown in Fig. 6. In general, higher processing temperature leads to an increase in the tensile properties of the PLA and ABS based composites. However, a decrease in tensile strength of PA based composites is observed when the processing temperature increases.

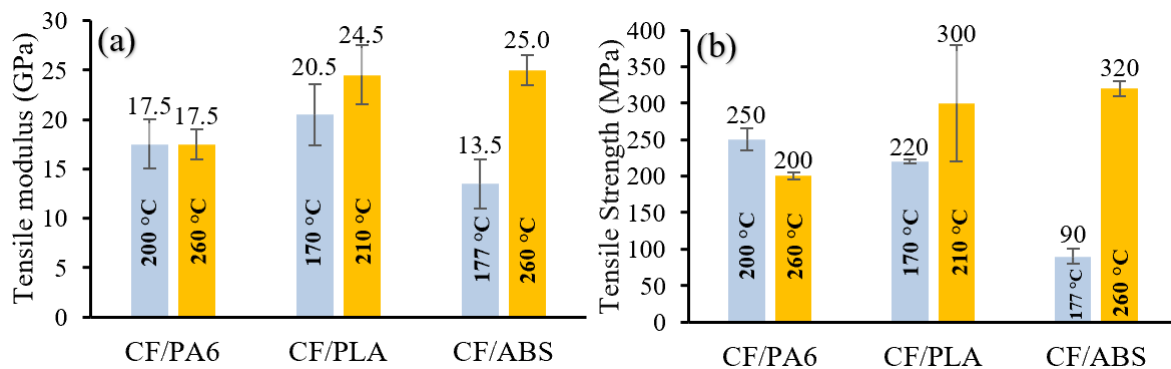


Fig. 6. Mechanical properties of FRCs fabricated using modified FDM processes at elevated temperatures: (a) tensile modulus; (b) tensile strength (data from [29, 34]).

On the other hand, researchers found that higher printing temperature sometimes weakened the mechanical properties. Ning et al. [38] reported that a moderate nozzle temperature of 220 °C (among temperatures ranged from 210 °C to 230 °C) produced CF/ABS with the highest modulus, strength and ductility. In Fig. 7(a), clear separations between adjacent printed beads and layers are observed at lower printing temperature (210 °C). Moreover, at a higher temperature of 230 °C, the number of pores (shown in Fig. 7(c)) increases significantly compared with that shown in Fig. 7(b) for 220 °C. Better interlayer bonding and fewer pores in specimens printed at 220 °C led to the highest mechanical properties of FDM-fabricated CF/ABS.

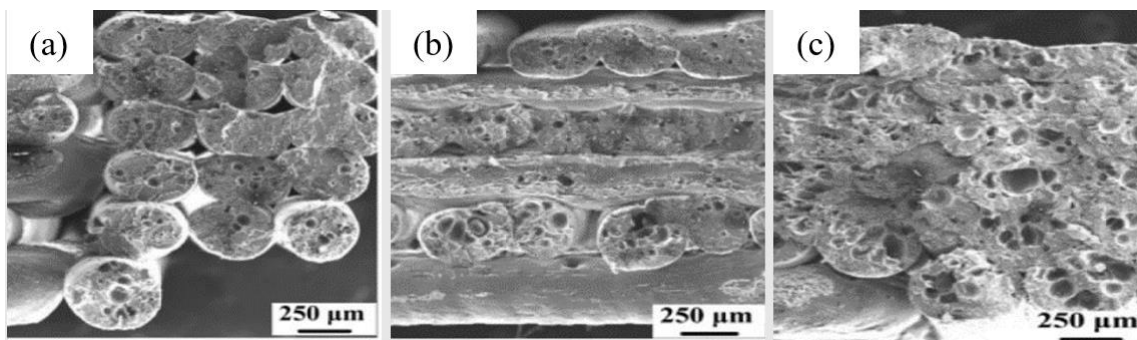


Fig. 7. Fracture interfaces of FDM-fabricated CF/ABS specimens printed at nozzle temperature of: (a) 210 °C; (b) 220 °C; (c) 230 °C [38].

2.2. DIW and the mechanical properties of DIW-fabricated discontinuous FRCs

2.2.1 Direct Ink Writing (DIW)

DIW is also an extrusion-based AM technique. While FDM uses solid filaments, DIW uses viscous inks as feedstock materials. DIW is less frequently used to fabricate discontinuous FRCs due to the following two reasons. Firstly, DIW can only process thermosets at room temperature, while UV or heat assisted treatment must be employed to process thermoplastics. Thermoplastics utilized in DIW are PLA [42] and PA [43]. Thermosets such as acrylic-based and thermally curable epoxy-based resins can be combined together to achieve an improved curing procedure [44]. Secondly, DIW is less preferable due to the fact that fibers cannot be

automatically aligned unless additional external forces are applied. Truby and Lewis [45] modified a standard DIW printer by adding a screw into the extruder to apply shear stress during the extrusion process. Well-aligned fibers were observed in the printed composites. The stiffness of the printed composites containing fibers aligned in the loading direction was nearly 10 times higher than that of many DIW-fabricated pure polymers. Shear induced treatment in the DIW process could be an efficient way to align fibers in the printing direction [46]. George et al. [47] reported approaches using a magnetic field to actively control the orientation of fibers, which inevitably introduced some complexity to the printing process.

2.2.2 Mechanical properties of DIW-fabricated discontinuous FRCs

Research on the mechanical properties of DIW-fabricated FRCs is limited. Nawafleh et al. [48] reported that the flexural modulus and strength of KF/EPON826 increased from 3.8 GPa and 78 MPa at 3.5% fiber volume fraction (V_f) to 4.2 GPa and 108 MPa at 6.3% V_f , respectively.

Invernizzi et al. [43] mixed photocurable resin with PA as the matrix so that UV light could assist the printing process as an additional curing source. Liquid phase PA with 33 wt.% and 50 wt.% of the photocurable resin was named B33 and B50, respectively. As expected, with the addition of CF and GF, both the tensile modulus and strength of the printed FRCs were improved. Moreover, CF composites exhibited better tensile performance than GF composites. Compared with pure B33, the tensile modulus (3.5 GPa) and strength (42 MPa) of GF/B33 were enhanced by approximately 35% and 20%, respectively. In contrast, the tensile modulus (3.9 GPa) and strength (31 MPa) of CF/B50 were improved by 44% and 94%, respectively, compared with pure B50.

In addition, Invernizzi et al. [43] found that sizing of CF filaments by cryogenic treatment increased the tensile modulus and strength of CF/B50 by approximately 10% because liquid nitrogen made the filaments' surface rougher resulting in enhanced bonding between fibers and

matrix layers, as shown in Fig. 8. The surfaces of untreated fibers (Fig. 8(a)) are relatively smooth. Conversely, the fiber surfaces after the sizing process are rougher (Fig. 8(b)). In addition, slippage and large amount of fibers pull-out can be observed at the fracture surface of untreated specimens, which indicates poor interfacial interaction between the fibers and matrix (Fig. 8(c)). However, stronger bonding between fibers and matrix is obtained upon sizing as demonstrated by the presence of a significant amount of residual matrix around the broken fibers (Fig. 8(d)). This is also the evidence that loads are successfully transferred to the fibers.

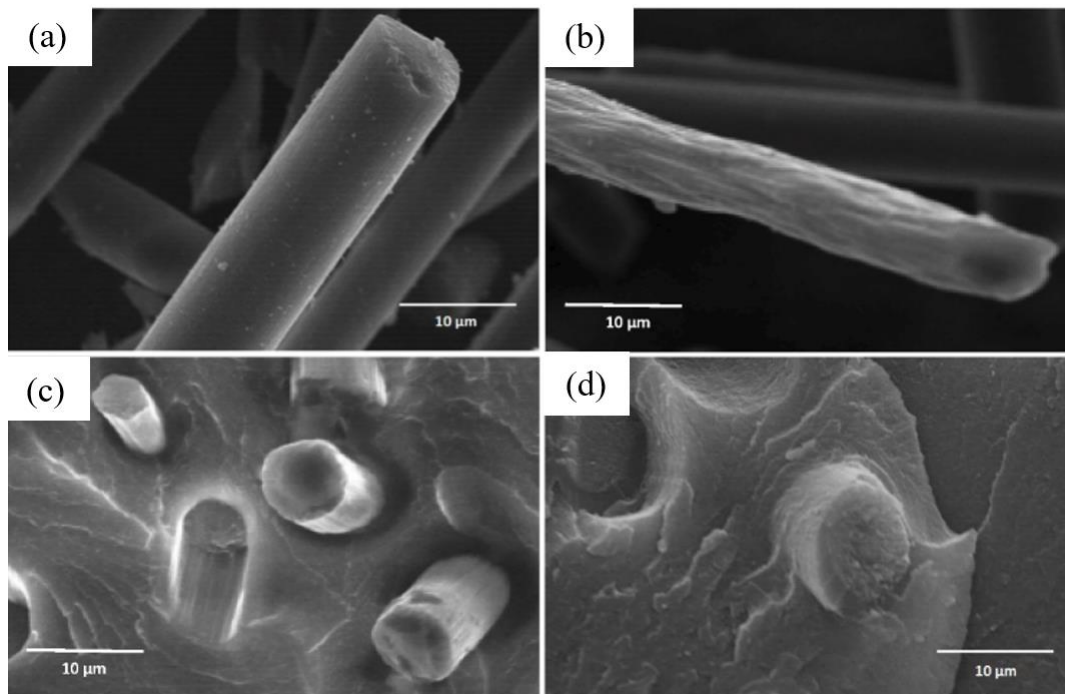


Fig. 8. SEM photographs of (a) untreated fibers; (b) nitrogen treated fibers; (c) fracture surface of untreated CF/B50; (d) fracture surface of treated CF/B50 [43].

2.3. SLS and the mechanical properties of SLS-fabricated discontinuous FRCs

2.3.1 Selective Laser Sintering (SLS)

SLS uses CO₂ laser as the heat source and fiber-reinforced powder and polymer as raw materials to fabricate FRCs. The ideal fiber size is between 20 µm and 80 µm. The distribution of fiber is expected to be as uniform as possible, both in terms of volume and number of fibers [49]. In order to fabricate fiber-reinforced powder for SLS process, carbon fibers and plastic

resins are firstly mixed in an organic solvent to produce a homogeneous mixture. This solvent is subsequently removed to precipitate out the powder, which is composed of carbon fiber and plastics. The powder is further crushed and milled. Since the fibers are relatively evenly compounded in the raw material before printing, the printed materials have similar mechanical properties in all directions (i.e., isotropy) [50]. Currently SLS is the only AM technique that can fabricate FRCs with multiple types of fibers and polymers in one component.

2.3.2 Mechanical properties of SLS-fabricated discontinuous FRCs

The most common polymer powders for SLS process are PA11 and PA12 [51]. Both PA11 and PA12 are Nylon-based materials with printing temperature at approximately 130 °C [52]. Compared with pure polymer materials, SLS-fabricated FRCs have superior properties such as higher mechanical strength, greater heat resistance, and better manufacturing accuracy. The SLS-fabricated discontinuous FRCs are as strong, flexible, and durable as FDM-fabricated ones.

Jansson and Pejryd [49] showed that the tensile strength of CF/PA12 fabricated in the printing direction was the highest, approximately 67 MPa, while the composites printed along the diagonal direction exhibited a lower tensile strength of approximately 31 MPa.

Similarly, the mechanical strength of SLS-fabricated FRCs increases with the increase of carbon fiber weight percentage. Yan et al. [51] found that the flexural strength of CF/PA12 increased from 76 MPa to 113 MPa when the CF percentage increased from 30 wt.% to 50 wt.%.

In addition, Goodridge et al. [53] investigated the tensile properties of SLS-fabricated carbon nanofiber-reinforced PA12 under dynamic loading. Commercialized PA12 was melted and compressed with 3 wt.% of carbon nanofibers (CNFs), which were further crushed into powder with an average size of 50 μm . The dynamic test performed at a frequency of 1 Hz

showed that the storage modulus of CNFs/PA12 was 1.2 GPa at 25 °C, which was 22% higher than that of the SLS-fabricated PA12.

Recent development in SLS printers has enabled the use of novel matrix materials such as PAEK and PEEK. Unlike PA-based powder, PEEK requires a much higher printing temperature at approximately 340 °C [54], which is challenging for SLS powder bed. Hoskins et al. [55] conducted a series of standard mechanical tests on pure PEEK using commercially available filaments purchased from EOS and found the tensile strength of 5 wt.% CF/PEEK was approximately 89 MPa, which was greater than that of SLS-fabricated PA12, and SLS-fabricated CF/PA12 composites. However, most research findings showed that the tensile strength of SLS-fabricated fiber-reinforced PEEK composites did not improve at all no matter what type of fibers (e.g., graphene, granite and carbon nanofibers) was added [56-58]. Only when Yan et al. [59] further increased the processing temperature to 380 °C, the tensile modulus and strength of 10 wt.% CF/PEEK composites increased to 7.5 GPa and 110 MPa, respectively, which was approximately 67% and 29% higher than those of SLS-fabricated pure PEEK.

In addition to employing new matrix materials, a novel method to improve the curing efficiency of SLS process was introduced by Zhu et al. [60]. The high-performance thermosetting epoxy (EP) was infiltrated into SLS-fabricated CF/PA12 parts and curing them at 150°C. The reinforcing CFs were well distributed in the PA12 (Fig. 9(a)) and the thermosetting epoxy was well infiltrated into voids between fibers and matrix (Fig. 9(b)). Mechanical test results also showed that the ternary CF/PA12/EP yielded ultimate tensile strength of 101 MPa and flexural strength of 153 MPa, which were higher than those of most SLS-fabricated FRCs using the normal SLS process.

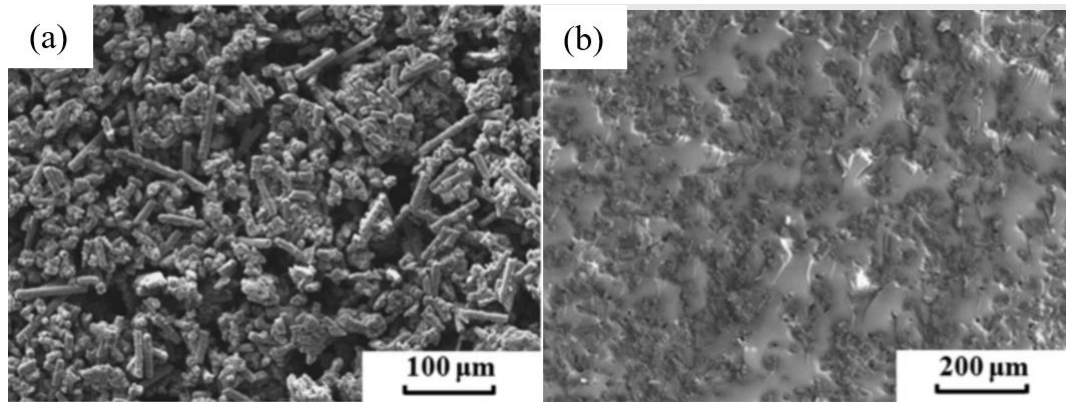


Fig. 9. SEM images of the cross-sectional surfaces of SLS-fabricated FRCs: (a) CF/PA12 parts as fabricated right after SLS process; (b) CF/PA12/EP ternary composite [60].

2.4. SLA and the mechanical properties of SLA-fabricated discontinuous FRCs

2.4.1 Stereolithography (SLA)

SLA is the first commercialized AM technique for rapid prototyping in the early 1990s [61] and has been applied to a wide range of industrial sectors. Fig. 10 [62] shows a typical SLA process to fabricate FRCs, where a focused laser is used to irradiate the surface of the light-cured material (which is mainly a photosensitive resin), so that it can complete the printing on one layer from point to line and line to surface. Such a printing process is repeated in sequence until the final product is fabricated. Once the printing is completed, high intensity ultra-violet (UV) light is applied to the SLA model to complete the polymerization process [63]. Among all AM techniques for discontinuous FRCs, SLA products have the best surface quality and the highest dimensional precision (up to approximately 50 μm) [64]. SLA-fabricated prototypes are directly generated from a CAD drawing, with a fast-processing speed, short production cycle, and no need for further machining to achieve the required dimensions and surface finish. However, the disadvantages of the SLA techniques are also evident. Firstly, the system is expensive and maintenance cost is high. Secondly, most of the resin is toxic and odorous. Therefore, a closed working environment is required. Thirdly, the operation of the software is complicated and requires a professional staff to operate it. Fourthly, the SLA-fabricated materials need more post processing such as washing and curing.

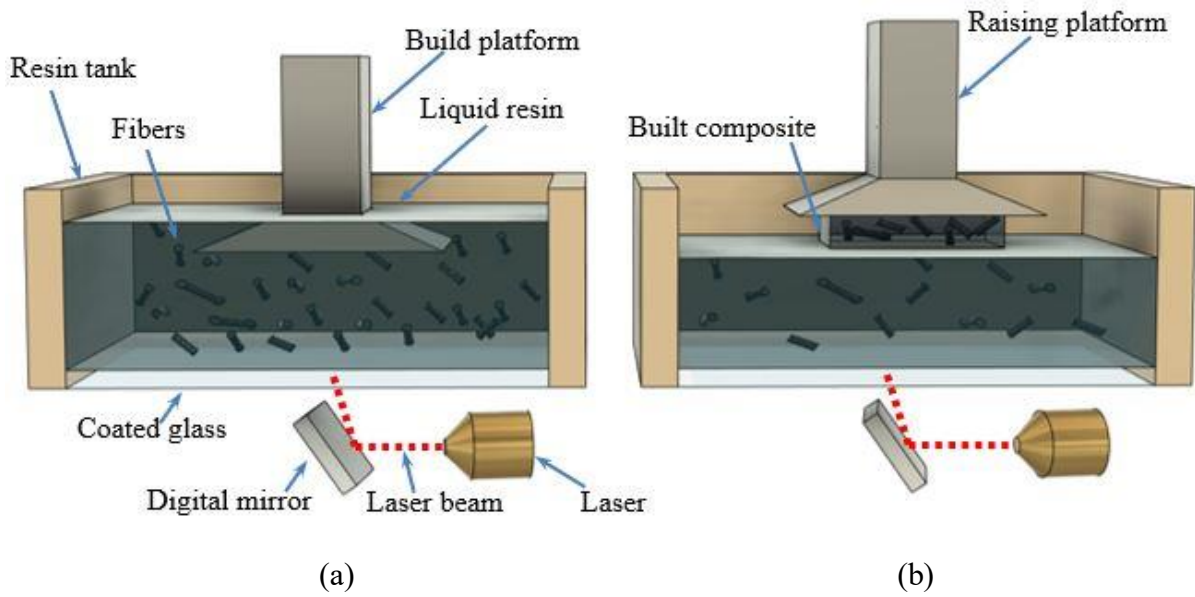


Fig. 10. Schematic diagram of SLA process to fabricate discontinuous FRCs: (a) initial stage of typical SLA printer; (b) raised platform with cured composites.

2.4.2 Mechanical properties of SLA-fabricated discontinuous FRCs

Nano reinforcement was reported to enhance the mechanical performance of SLA-fabricated composites. For instance, an improvement in tensile strength from 74 MPa to 82 MPa was achieved by adding cellulose nanocrystals (CNCs) into neat stereolithography resins (SLRs) [65]. Tensile strength increased from 46 to 54 MPa by employing nano SiO₂ without influencing the printing resolution [66], and the tensile strength was tripled (from 20 MPa to 60 MPa) by adding 1 wt.% graphene oxide (GO) to Formlabs' grey resin and annealing at 100 °C [67]. Although nanofibers were the main reinforcement to strengthen SLA-fabricated composites, e-glass fibers with 1.6 mm length (milli-fibers) could also be added to urethane acrylic-based photopolymer [68].

Sano et al. [62] conducted comprehensive mechanical tests on glass fiber-reinforced light-cured resin composites. The tensile modulus remained the same as 0.2 GPa when the fiber weight percentage changed from zero to 20 wt.%, and increased to 0.4 GPa, 0.5 GPa and 1 GPa when the fiber weight percentage changed to 30 wt.%, 40 wt.% and 50 wt.%, respectively. On

the other hand, the tensile strength of the composites increased monotonically with the fiber weight percentage. The highest tensile strength obtained was 22 MPa, which was double the tensile strength of the matrix only. These results were obtained with powder sized fibers (less than 10 μm). Sano et al. [62] pointed out that using chopped glass fibers of millimeter scale in SLA-fabricated FRCs was considered unsuccessful because the fibers cannot be self-oriented, and fibers were only observed in the top layers (Fig. 11(a) and (c)) and no fiber was observed in the bottom layers (Fig. 11(b) and (d)).

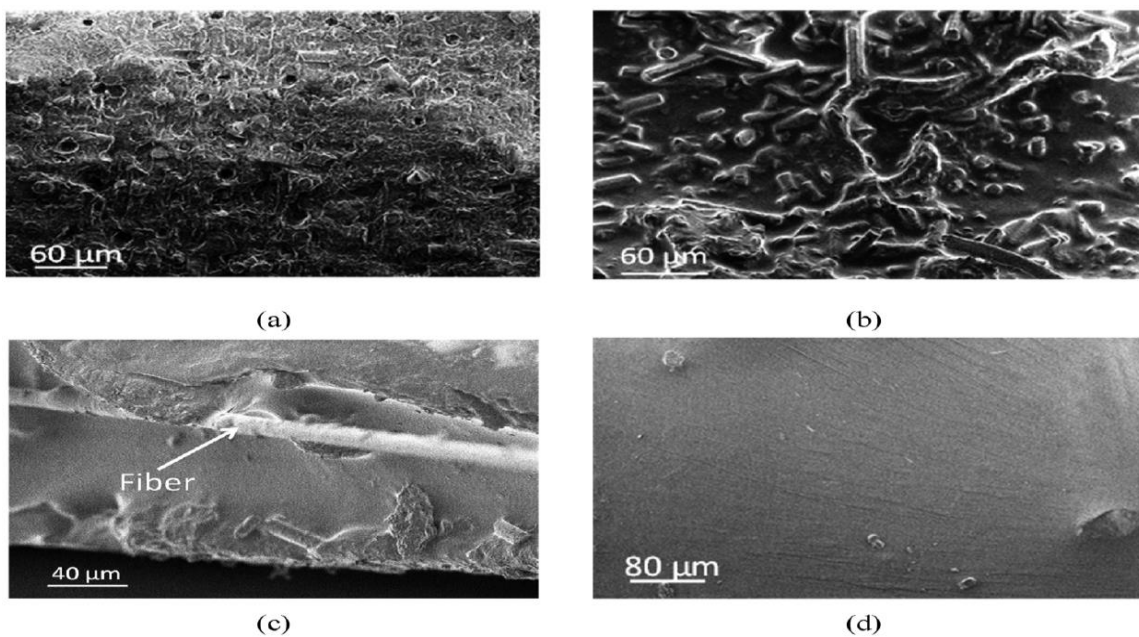


Fig. 11. SEM images of the cross sections of SLA-fabricated specimens: (a) top layer of the cross section of a glass powder specimen; (b) bottom layer of the cross section of a glass powder specimen; (c) top layer of the cross section of a short glass fiber specimen; (d) bottom layer of the cross section of a short glass fiber specimen [62].

2.5. Comparison of the mechanical properties of discontinuous FRCs fabricated using FDM, DIW, SLS and SLA

Fig. 12 summarizes the tensile properties of discontinuous FRCs manufactured by FDM, DIW, SLS and SLA. Overall, FDM-fabricated FRCs exhibit good mechanical properties (Regions 1.1 and 1.2). It is noteworthy that for modified FDM (Region 1.2) technique (i.e., HPDF method), after increasing the production temperature and adding a consolidation step

during filaments preparation, the tensile modulus and tensile strength of the printed composites can be over 20 GPa and 200 MPa respectively. On the other hand, DIW-fabricated FRCs (Region 2) have relatively low tensile modulus (3.5 to 4.4 GPa) and tensile strength (16 to 42 MPa) due to the challenges to align fibers (i.e., random fiber orientations). The tensile modulus (2.1 to 8.9 GPa) and strength (31 to 109 MPa) of SLS-fabricated FRCs (Region 3) are similar to those of FDM-fabricated FRCs. The average tensile modulus (0.9 GPa) and tensile strength (29 MPa) of SLA-fabricated FRCs are the lowest among those fabricated by other AM techniques (Region 4).

Since the most popular traditional method to produce FRCs is injection molding with polypropylene (PP) and Polyamide (PA) as matrix materials [69], the mechanical properties of injection molded discontinuous fiber-reinforced PP and PA are also plotted in Fig. 12 for comparison with AM-fabricated FRCs [69-71]. The average tensile modulus and strength of discontinuous fiber-reinforced polypropylene (PP) are approximately 17 GPa and 125 MPa [72,73]. Verdejo de Toro et al. [74] made a direct comparison between FDM-fabricated and injection molded CF/PA6. The tensile modulus and strength of FDM-fabricated CF/PA6 were 6.2 GPa and 52 MPa, while they were 7.5 GPa and 65 MPa for injection molded CF/PA6. Hassan et al. [75] tensioned injection molded CF/PA66 composites and obtained tensile moduli ranging from 13 GPa to 29 GPa, and tensile strengths from 124 MPa to 173 MPa, when the CF volume percentage increased from 21% to 32%, which indicated that injection molded specimens have better tensile properties than standard AM-fabricated FRCs (excluding modified FDM-fabricated FRCs). However, data in Regions 1.2 and 5 manifest that the modified FDM fabricated CF/PAs possess higher tensile strength than injection molded CF/PA.

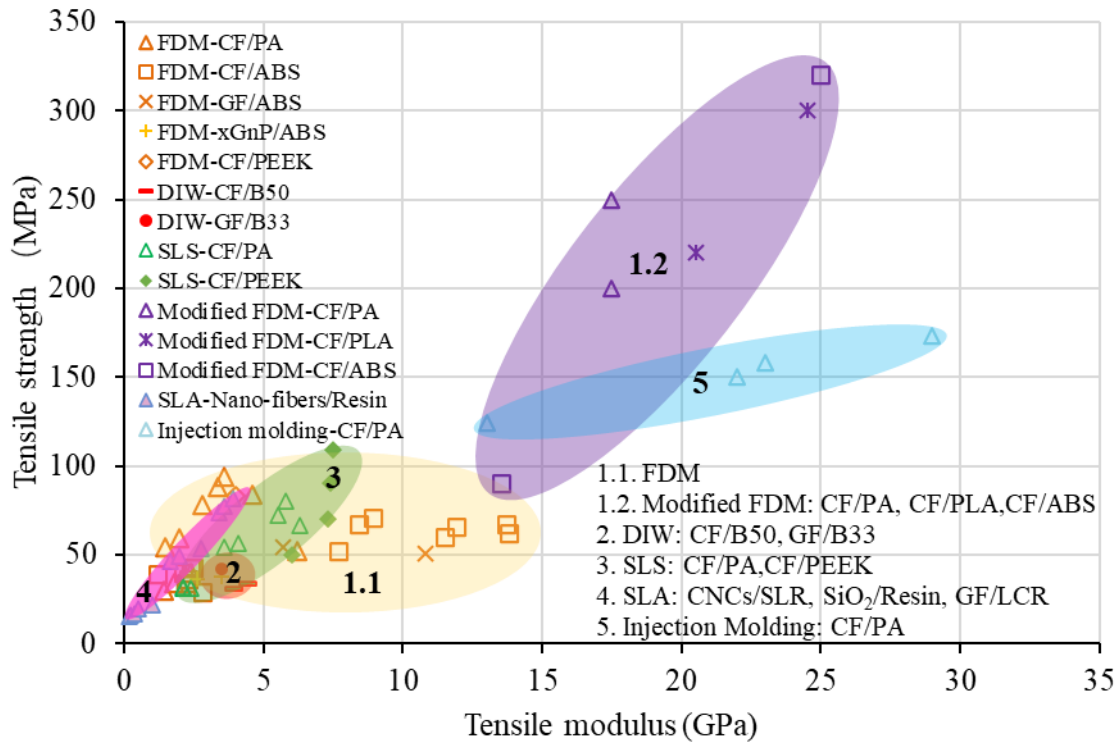


Fig. 12. Tensile strength vs. tensile modulus of materials manufactured via various AM techniques and traditional injection molding (data from [25, 26, 29, 30, 43, 49, 62, 69-78]).

3. Continuous FRCs: AM techniques and resulting mechanical properties

AM techniques developed to use continuous fibers have been advanced in the past five years [5]. Continuous fiber reinforcements significantly improve the mechanical properties of composites compared with discontinuous fibers. However, there are only three AM techniques (FDM, SLA and LOM) available to utilize continuous fibers. Various fibers can be employed but CF, GF and KF are the most common fibers used for all these three AM techniques. However, different AM techniques require different forms of fibers. Dry fiber filaments and sized prepreg fiber filaments coated with matrix are used for FDM technique [79]; woven or non-woven fiber mats are suitable for SLA technique [80, 81]; and LOM technique utilizes fiber sheets [82, 83]. The mechanical properties and parameters that affect the mechanical performance of continuous FRCs fabricated by FDM, SLA and LOM techniques are discussed in the following subsections.

3.1. FDM and the mechanical properties of FDM-fabricated continuous FRCs

3.1.1 Fused Deposition Modeling (FDM)

Most continuous FRCs are fabricated by FDM because it is simple to operate and cost efficient [6]. FDM technique for continuous fibers can be divided into two categories, depending on how the fiber filaments are fed. The reinforcing fibers can either be incorporated through coaxial extrusion [84-88] or dual extrusion [89-93]. Fig. 13(a) [94] shows a schematic of coaxial extrusion of continuous FRCs using a single extruder. When the nozzle is heated, the molten thermoplastic material is layered before depositing of reinforcing filaments. As soon as the first layer of thermoplastic material is deposited on the building platform, the reinforcing fibers are extruded, attached and solidified onto the previous polymer layer. After completing the first layer, the fiber and polymer filaments are injected into the extruder simultaneously in the subsequent printing sequences [3]. On the other hand, Fig. 13(b) [95] shows a schematic of the printing process using a dual extrusion FDM printer. This dual-extruder system allows the reinforcement in selected individual layers. In addition, since the polymer and fiber are separately extruded onto the platform, two nozzles do not necessarily move simultaneously and certain areas can be specially reinforced, which enables users to design the printing process to achieve desirable performance to fulfill customers' needs [6, 7].

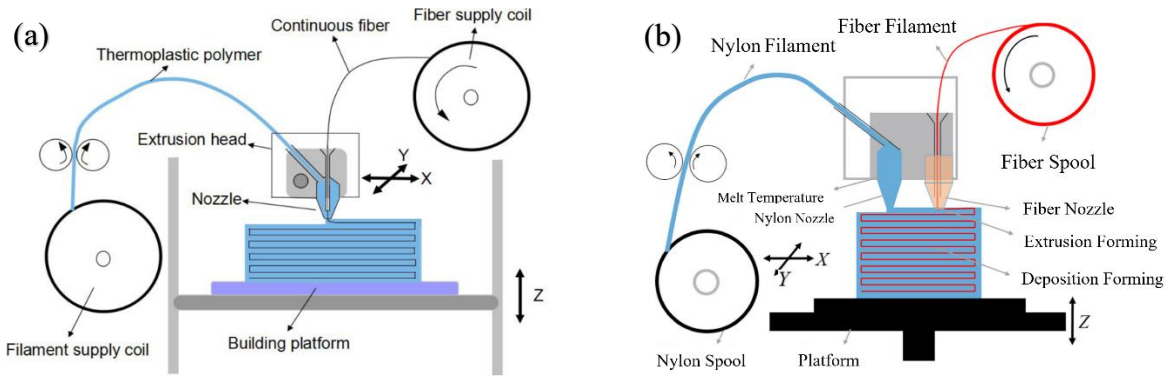


Fig. 13. FDM printing process to fabricate continuous FRCs: (a) coaxial extrusion using a single nozzle [94]; (b) dual extrusion using two nozzles [95].

3.1.2 Mechanical properties of FDM-fabricated continuous FRCs

The mechanical properties of continuous FRCs vary with fiber type and treatment of fiber filaments, fiber volume fraction, matrix, stacking sequence, infill pattern and external compaction.

3.1.2.1 The effect of fiber type and treatment of filaments

In order to understand the properties of composites, the properties of parent materials (fiber or matrix) are expected to be known. Peng et al. [96] tensioned the raw carbon fiber filaments supplied by Markforged and found that the tensile modulus and strength of continuous carbon fiber filaments at failure were 97 GPa and 1366 MPa, respectively, which were 80% and 70% higher than those of their composite counterparts.

Fig. 14 presents the mechanical test data obtained directly from Markforged for composite with approximately 40% V_f continuous fibers oriented along loading direction [77]. CF/PA has the highest tensile and flexural strengths, followed by KF/PA, and GF/PA has the lowest tensile and flexural strengths. The tensile strength of CF/PA (800 MPa) was almost 10 times that of composites with discontinuous fibers (approximately 80 MPa). In addition, several research groups conducted their own tests utilizing 3D printers and materials provided by

Markforged and obtained slightly different results. For example, Justo et al. [90] reported that the tensile modulus and strength of 40% Vf CF/PA composites were 68 GPa and 701 MPa respectively, while the tensile modulus and strength of 50% Vf GF/PA were 26 GPa and 575 MPa respectively, which manifested CF's superior reinforcement than GF. In terms of flexural properties [89], by employing 11% Vf fibers, CF/PA composites showed the highest flexural modulus and strength of 13 GPa and 250 MPa respectively. The flexural modulus of 10% Vf GF/PA composite (4.2 GPa) was lower than that of KF/PA composite (6.7 GPa), while the flexural strength of 10% Vf GF/PA composites (197 MPa) was greater than that of KF/PA (126 MPa).

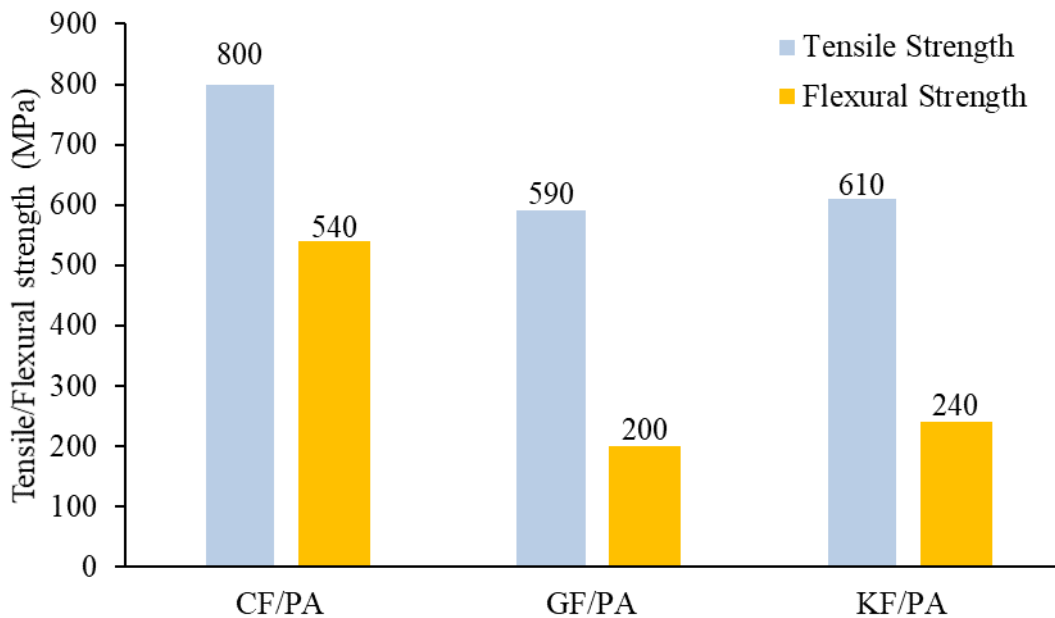


Fig. 14. Tensile and flexural strengths of FDM-fabricated 40% Vf fiber-reinforced PA composites (data from [77]).

Most experimental tests conducted on AM-fabricated continuous FRCs were under quasi-static loading conditions. The only impact test conducted to date is the Charpy impact test [97-99]. Due to the brittle nature of CF, 24.9% Vf CF/PA composite exhibited the lowest storage energy (33 kJ/m²), followed by 29.5% Vf KF/PA (84 kJ/m²), and 29.2% Vf GF/PA with the highest resistance to the impact (207 kJ/m²) [97].

Pertuz et al. [100] evaluated the fatigue properties of AM-fabricated nylon composites reinforced with three different continuous fibers (CF, GF and KF). CF/Nylon showed superior fatigue properties comparing with GF/Nylon and KF/Nylon.

The quality of fabricated fiber filaments affects the bonding between fibers and matrix and thus influences the overall properties of AM-fabricated continuous FRCs. The interfacial bonding between matrix and raw fibers in AM-fabricated composites is normally not very good [101]. With the innovation of production techniques, the sizing process was recently applied to manufacture impregnated filaments, and high temperature extruder was also introduced to completely melt the sizing agent to improve the bonding strength between fibers and matrix [102]. Attempts were also undertaken to modify the surface of carbon fiber bundles by coating them with PLA before the printing process to improve the interfacial strength of fibers and matrix [91]. The effect of sizing can be observed in Fig. 15 as improved infiltration of PLA resulted in homogeneous distribution of PLA between the surface-modified fibers, nearly void-free microstructure (Fig. 15(c)), and the presence of residual PLA around pulled out fibers (Fig. 15(d)). Hence, the tensile strengths of PLA, reinforced PLA without and with surface-modified carbon fibers were 28 MPa, 80 MPa, and 91 MPa respectively, and the flexural strengths were 53 MPa, 59 MPa, and 156 MPa respectively [91]. Plasma, HNO₃ and O₃ have also demonstrated to successfully modify the fiber surface [103, 104]. It is worth noting that in 2016 Markforged released its latest desktop printer, Mark Two, and all the fiber filaments provided by Markforged are sized and coated with PA since then.

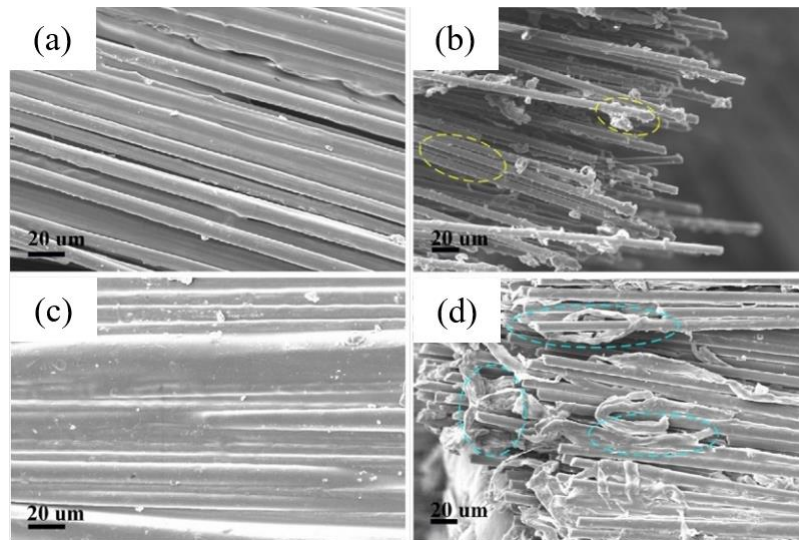


Fig. 15. SEM micrographs of AM-fabricated continuous FRCs: (a) fiber-matrix interface of CF/PLA; (b) fiber pull-out phenomenon of CF/PA after a tensile test; (c) fiber-matrix interface of modified CF/PLA and (d) fiber pull-out of modified CF/PLA after a tensile test [91].

3.1.2.2 The effect of fiber volume fraction

Increasing carbon fiber volume fraction in CF/PA [89, 90, 93], CF/PLA [105], CF/Onyx [96] resulted in improved tensile and flexural properties. For example, for CF/PA with 6% Vf and 18% Vf CF/PA, the tensile moduli were 14 GPa and 36 GPa respectively, and tensile strengths were 140 MPa and 464 MPa [93]. In general, both tensile modulus and strength of CF/PA increase with CF volume fraction, as shown in Fig.16. The mechanical properties of GF and KF reinforced composites show a similar trend. Dickson et al. [89] found that the tensile modulus and strength of GF/PA increased from 3.1 GPa to 3.8 GPa, and 194 MPa to 206 MPa when the GF volume fraction increased from 8% to 10% Vf. The tensile modulus and strength of KF/PA increased from 3.6 GPa to 4.4 GPa, and 150 MPa to 164 MPa when the KF volume fraction increased from 8% to 10% Vf [89]. Melenka et al. [92] also reported that the tensile modulus and strength were enhanced from 1.8 GPa to 9.0 GPa, and 31 MPa to 84 MPa when the KF volume fraction increased from 4% to 10% Vf.

Flexural modulus and strength also increase with fiber volume fraction [89,106]. Dickson et al. [89] found that the flexural modulus and strength of GF/PA increased from 3.9 GPa to 4.2 GPa, and 166 MPa to 197 MPa when the GF volume fraction increased from 8% to 10% Vf. The flexural modulus and strength of KF/PA composites increased from 4.6 GPa to 6.7 GPa, and 107 MPa to 126 MPa when the KF volume fraction increased from 8% to 10% Vf [89]. Araya-Calvo et al. [106] showed that the flexural moduli of CF/PA were 5.2 GPa, 8.9 GPa and 14.2 GPa, and flexural strengths were 84 MPa, 143 MPa and 231 MPa when the CF volume fractions were 17.18%, 32.19% and 48.93% Vf, respectively.

Araya-Calvo et al. [106] also found that increasing carbon fiber volume fraction in CF/PA resulted in an improvement in their compressive properties. The compressive modulus increased from 1.5 GPa to 2.1 GPa, and compressive strength altered from 40 MPa to 53 MPa when carbon fiber volume fractions increased from 8.18% to 24.44%. In addition, Justo et al. [90] obtained a compressive modulus of 53 GP with 41% Vf CF/PA, which was similar to the data provided by Markforged [77], but their compressive strength (223 MPa) was lower than Markforged's (320 MPa).

In addition. shear strength of continuous FRCs increases with fiber volume fraction. Caminero et al. [107] found that increases in shear strength for various FRCs from 22.2 MPa to 31.9 MPa (CF/PA), 13.9 MPa to 21.0 MPa (GF/PA) and 13.7 MPa to 14.3 MPa (KF/PA), when fibers volume fractions increased from approximately 27% to 73%.

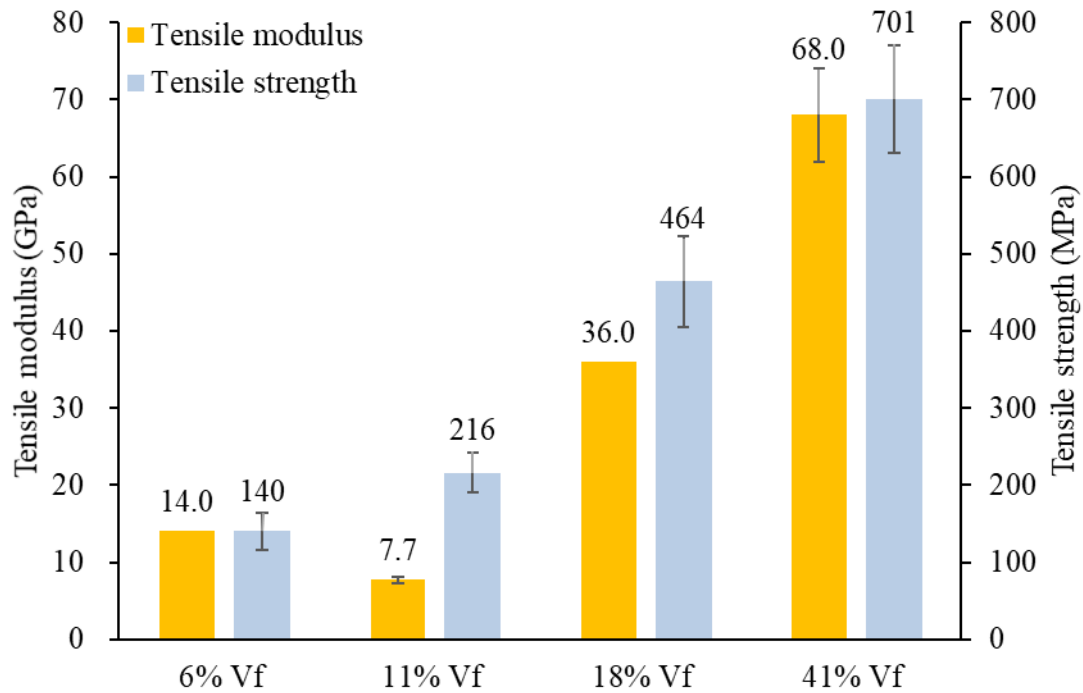


Fig. 16. The effect of fiber volume fraction on the tensile properties of CF/PA (data from [89, 90, 93]).

3.1.2.3 The effect of matrix

The commonly used matrix materials for FDM include PA [77, 89, 90, 92, 93, 97, 106-110], PLA [91, 101], ABS [94], Onyx [96, 111, 112], PEEK [98] and PP [113]. Onyx is a type of 15 wt.% discontinuous carbon fiber reinforced PA6 material which offers high strength, toughness, and chemical resistance. It can be printed alone as discontinuous FRCs or be reinforced with continuous CF or GF or KF to fabricate continuous FRCs. Markforged dual extrusion printers [114] with two nozzles can only use PA and Onyx, while other printers with a single nozzle can utilize PA, PLA and ABS.


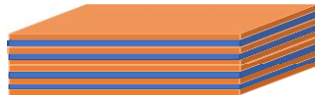
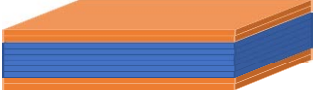
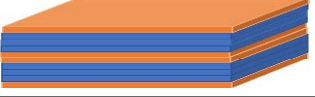
With 10 wt.% CF, the reported tensile modulus and strength were 20.6 GPa and 256 MPa for CF/PLA [99], which were greater than 4.2 GPa and 147 MPa for CF/ABS [94]. Moreover, with 30% Vf CF, the tensile modulus and strength of CF/PLA were 49.1 GPa and 393 MPa [115], higher than those reported (25 GPa and 330 MPa) for 30.1% Vf CF/Onyx [96]. However, in another study, the tensile modulus and strength were 60.9 GPa and 780 MPa for 27% Vf

CF/Onyx, respectively [111]. Such diverse tensile properties reported by different researchers may be attributed to the following two factors: (1) the printer might be different. Peng et al. [96] used a Markforged X printer, while Iragi et al. [109] used a Markforged Mark Two printer. (2) the geometries and sizes of the tested specimens employed by the above two research groups were different.

3.1.2.4 The effect of stacking sequence

The effect of stacking sequence on the mechanical behavior of FDM-fabricated continuous FRCs was studied in [96]. Table 3 shows the four types of stacking sequences of FRCs with four and six CF layers, respectively. Results from [96] showed that the tensile strength of 30% Vf CF/Onyx specimen was better with separated CF layers (342 MPa) than with centered CF layers (317 MPa). This was attributed to the occurrence of three different types of interfaces and their relative amount: namely the interface between adjacent carbon fibers (C-C), the interface between carbon fibers and matrix (C-S), and the interface between printed matrix lines (S-S), as shown in Fig. 17(a). After the tensile tests, delamination at the C-C interfaces was easily observed (Fig. 17a), whereas much fewer debonding was found at C-S or S-S interfaces as shown in Fig. 17(b). Specimens with separated carbon fiber layers had more S-S and C-S interfaces with better interfacial strength, resulting in higher tensile properties.

Table 3 Tensile modulus and strength of FDM-fabricated FRCs with different configurations of CF layers (blue color) and matrix layers (orange color) (data from [96])

Materials (30% Vf CF/Onyx)	Stacking sequence	Tensile modulus (GPa)	Tensile strength (MPa)
4CF-centered		25	317
4CF-separated		25	342
6CF-centered		36	451
6CF-separated		39	516

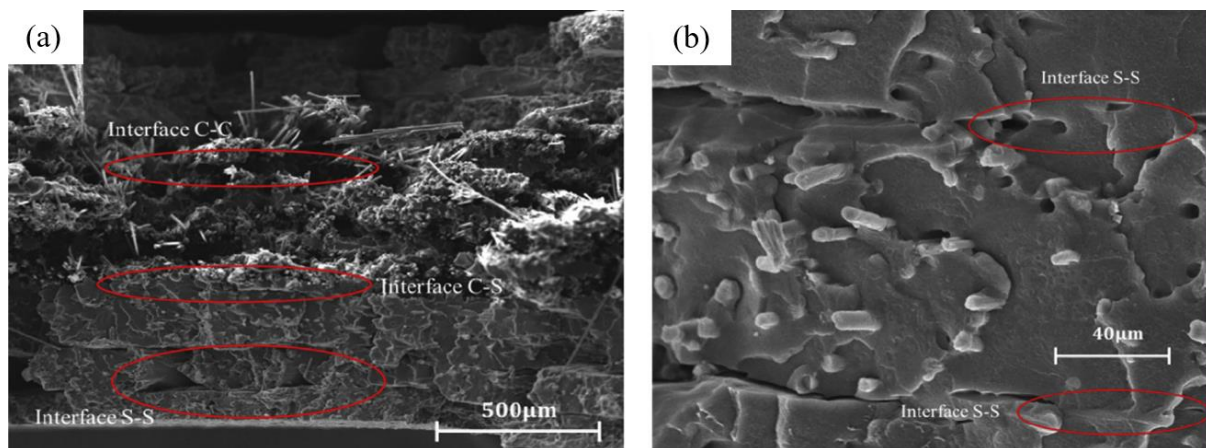


Fig. 17. SEM images of the tensile fracture surfaces of (a) FRCs with 4CF-centered; (b) FRCs with 4CF-separated showing interfaces (S-S) between printed matrix lines [96].

3.1.2.5 The effect of infill pattern

One advantage of additive manufacturing of composite is the feasibility to print parts with complex hollow interior features, such as triangular, rectangular, cubic, honeycomb and gyroid infills [116]. The above-mentioned infill patterns are available for matrix materials and can be printed with different densities, while only isotropic and concentric patterns can be selected for fibers. In addition, the investigation of the mechanical response of AM-fabricated FRC

structures using continuous fibers such as tubes, panels and cells are in its infancy has just started [117-120]. Mei et al. [121] conducted research on continuous FRCs with different types of matrix (Nylon) infill. They obtained the highest tensile modulus and strength for the composites with rectangular infill, followed by rectangular infill and hexagon infill. Araya-Calvo et al. [106] explored the effect of fiber infill pattern and obtained the highest compressive and flexural moduli (2.1 GPa and 5.4 GPa, respectively) for CF/PA with the concentric fiber infill pattern.

Brooks et al. [122] investigated the fatigue properties of continuous CF/PLA composites with the same volume fraction of CF, while different matrix infill densities of 25% and 90%, respectively. The results showed 25% infill CF/PLA had a better fatigue life, failing at 400 cycles, while CF/PLA with 90% infill density failed within 300 cycles.

3.1.2.6 The effect of external compaction

Compaction during 3D printing was developed to prevent the formation of a large number of voids in the printing process and increase the interfacial shear strength between printed lines [123,124]. One method is to install a programmable and heated compaction roller in FDM printers [88,125]. In the FDM process with compaction (Fig. 18), thermoplastic filaments and continuous carbon fibers are separately supplied to the 3D printer, and fibers are impregnated with the filament inside the heated nozzle before printing. The compaction roller is equipped with the printer head to consolidate a continuous fiber-reinforced layer right after the extrusion of impregnated filament. This significantly reduced the number of voids of the printed material which resulted in tensile strengths over 1 GPa [110].

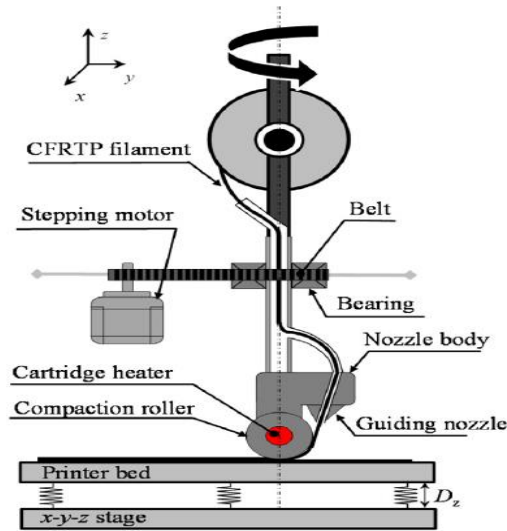


Fig. 18. A sketch of the developed printer head with a compaction roller [110].

Zhang et al. [125] obtained significantly enhanced tensile (645 MPa versus 110 MPa) and flexural (401 MPa versus 163 MPa) strengths for CF/PLA, with compaction than without pressure. Ueda et al. [110] compared both the tensile and flexural properties of CF/PA by 3D compaction printing (3DCP) and conventional FDM. The tensile moduli were the same (71.2 GPa), while the tensile strength of the 3DCP specimen (1031 MPa) was approximately 33% higher than that of the conventional FDM-fabricated specimen (777 MPa). SEM analysis revealed that this was due to the lower void volume fractions in 3DCP (3%) than in conventional FDM (10%) specimens. Likewise, Omuro et al. [115] showed that both the tensile modulus (63.9 GPa) and tensile strength (536 MPa) of the compacted CF/PLA were more than 30% higher than those of non-compacted CF/PLA. The flexural strength of compacted CF/PLA was also increased by approximately 40%, while the flexural modulus remained unchanged.

3.2. SLA and mechanical properties of SLA-fabricated continuous FRCs

Limited literature was found on SLA techniques to produce continuous FRCs [62, 126, 127]. Continuous fibers can be as either fiber filament bundle or woven fabric. Sano et al. [62]

employed continuous GF woven fabric as a reinforcing material. The tensile modulus and strength of GF/Light Cured Resin (LCR) were 1.8 GPa and 79 MPa respectively, which were approximately 7.2 and 11.5 times that of the parent resin. However, the tensile strength of SLA-fabricated continuous FRCs was much lower than that of the FDM-fabricated continuous FRCs. SEM analysis showed that the SLA process did not produce any large voids, but there was a large amount of fiber pull-out, which was attributed to the low interfacial strength between the fibers and resin in SLA-fabricated composites and resulted in low tensile strength.

Lu et al. [126] obtained a 24% increase in tensile modulus for SLA-fabricated CF/Accura60 compared with the parent Accura60 resin. However, the tensile modulus and strength of CF/Accura60 are less than those of GF/LCR.

Karalekas [127] compared the tensile properties of SLA-fabricated composites with nonwoven mats of PAN-based CF, E-Type GF, and KF reinforced acrylic resin (Ar) and epoxy resin (Er). For Ar-based composites (CF/Ar and GF/Ar), both tensile modulus and strength increased with the fiber mat nominal area weight (Table A2). Higher tensile properties were achieved with a fiber mat nominal area weight of 17 gm⁻² than that of 7 gm⁻². On the contrary, for Er-based composites, both tensile modulus and strength decreased with fiber nominal area weight due to poor bonding strength between adjacent resin and fibers mat.

3.3. Mechanical properties of LOM-fabricated continuous FRCs

Fig. 19 depicts a typical LOM fabricating process, which is similar to the conventional autoclave consolidation process [128, 129]. The fiber-reinforced prepreg sheets are firstly cut to a customized 2D shape by a laser cutter. The customized 2D shape prepreg layer is subsequently laid down onto the previously printed layers. Finally, the prepreg sheets are heated by laser and consolidated layer by layer via a heated compaction roller.

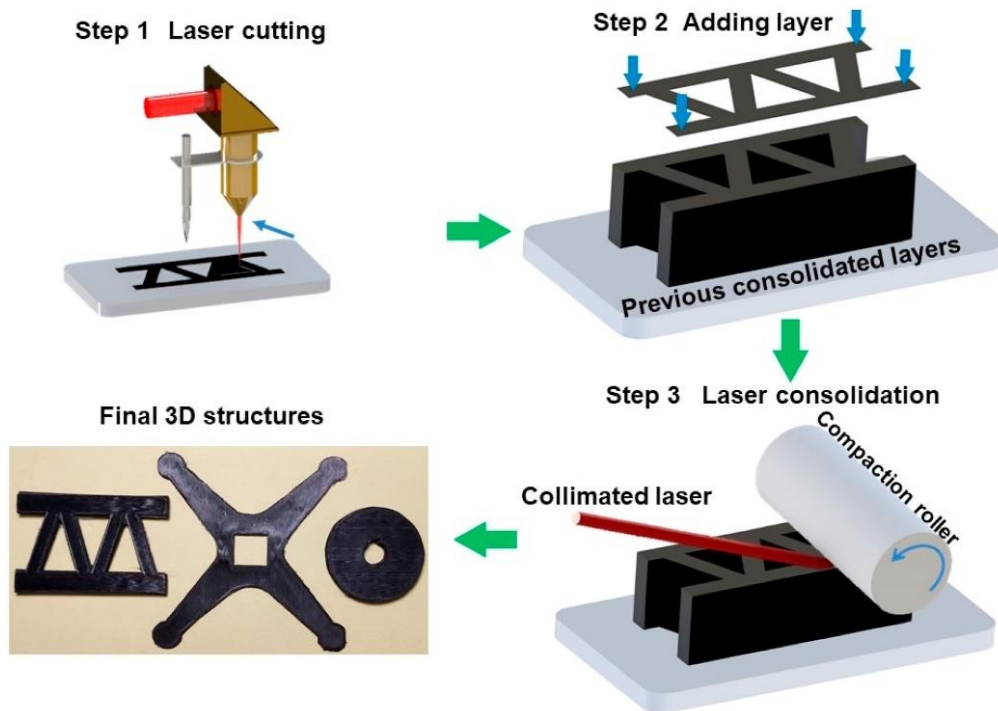


Fig. 19. Schematic of a LOM process to fabricate CF/PEEK [130].

Chang et al. [130] employed a novel method by adding a hot-press procedure when layering carbon fiber-reinforced PEEK prepreg composite sheets. The LOM-fabricated unidirectional 59% Vf CF/PEEK exhibited ultrahigh tensile modulus (133.1 GPa) and strength (1514 MPa), which were 17% and 25% higher than those fabricated without hot-press procedure. The flexural modulus and strength of the untreated composite were 89.7 GPa and 671 MPa, respectively. With hot-press treatment, the flexural modulus of the CF/PEEK composite was 40% higher than the original untreated composite, and the flexural strength was improved by 1.8 times. Recently, Chang et al. [131] added an ultrasonic vibration function to their original compaction roller to allow the compaction and vibration to take place at the same time during printing. The unidirectional CF/PA6 with 49% Vf fibers displayed an ultra-high tensile modulus of 106 GPa and an ultimate tensile strength of 1760 MPa. Micro-CT analysis unveiled that ultrasonic treatment reduced the voids in CF/PA6 to 1.6% from 15%- 22% in typical AM-fabricated FRCs [132].

Klosterman et al. [133] processed aerospace-grade prepreg E-glass fibers (52%-55% Vf) with epoxy matrix using LOM method. An additional hot-press cycle was also employed to fully consolidate LOM-fabricated GF/Epoxy. The achieved tensile, flexural and compressive strengths were 713 MPa, 1190 MPa and 896 MPa respectively. The mechanical properties of LOM-fabricated composites offered great potential applications in the automotive and aerospace industries due to their high degree of automation, ability of mass production and high mechanical properties of printed parts. Furthermore, Parandoush et al. [134] used the same technique to manufacture CF/PA6 with tensile strength of 668 MPa due to superior interfacial bonding.

3.4. Comparison of the tensile properties of continuous FRCs manufactured via different AM techniques

Since there are limited data of flexural and compressive properties of AM-fabricated continuous FRCs, the comparison is made only for tensile properties of AM-fabricated continuous FRCs. Fig. 20(a) maps the tensile properties of various continuous FRCs fabricated by FDM (yellow area), SLA (purple area) and LOM (green area) techniques. The map facilitates the selection of additive manufacturing techniques to produce continuous FRCs with desirable properties. The manufacturing method has a noticeable effect on the mechanical properties of continuous FRCs. The purple area shows SLA-fabricated continuous FRCs usually have low tensile modulus and strength. On the other hand, the yellow area in Fig. 20(a) represents the tensile properties of FDM-fabricated continuous FRCs with different fiber/matrix combinations. The tensile moduli range from approximately 3 GPa to 70 GPa, while tensile strengths range from 60 MPa to 1031 MPa. In addition, LOM-fabricated continuous FRCs exhibit remarkably high tensile strengths (668 – 1514 MPa), while the tensile

moduli vary from 18 GPa (for CF/PA6) to 133 GPa (for CF/PEEK). This may be because PA6 is a recycled matrix material and may not be able to bond well with fibers.

Fig. 20(b) shows the tensile strength versus fiber volume fraction of continuous FRCs fabricated by different AM techniques. Major observations are as follows.

- Tensile strength increases with fiber volume fraction for continuous FRCs fabricated by all three AM techniques (i.e., FDM, SLA and LOM).
- For FDM-fabricated continuous FRCs, CF reinforced composites show higher tensile strength than GF and KF continuous FRCs (Fig. 20(b), Regions 1, 2 and 3).
- As shown in Regions 4.1 and 4.2, the tensile properties of CF/PLA can be improved significantly after external compaction.
- FDM-fabricated FRCs (Regions 1, 2 and 3) display enhanced tensile strength compared with CFRCs fabricated by the conventional compression molding (Region 6).
- In addition, recent progress in LOM technique enables remarkable improvements in the tensile strength of LOM-fabricated composites (up to 1300 MPa shown in Region 5), which provides AM-fabricated continuous FRCs an opportunity to replace composites produced by the traditional compression molding process [14,135].
- Although the use of continuous fibers greatly enhances the mechanical properties of AM-fabricated composites, pressure and high temperature are not able to be applied during the AM fabricating process. Therefore, the mechanical properties of AM-fabricated composites are still inferior to those fabricated by traditional autoclave process (Region 7).
- The mechanical properties of the AM-fabricated discontinuous FRCs (Region 8) are better than the pure matrix, but they are inferior to those of the conventionally manufactured composites as well as AM-fabricated continuous FRCs.

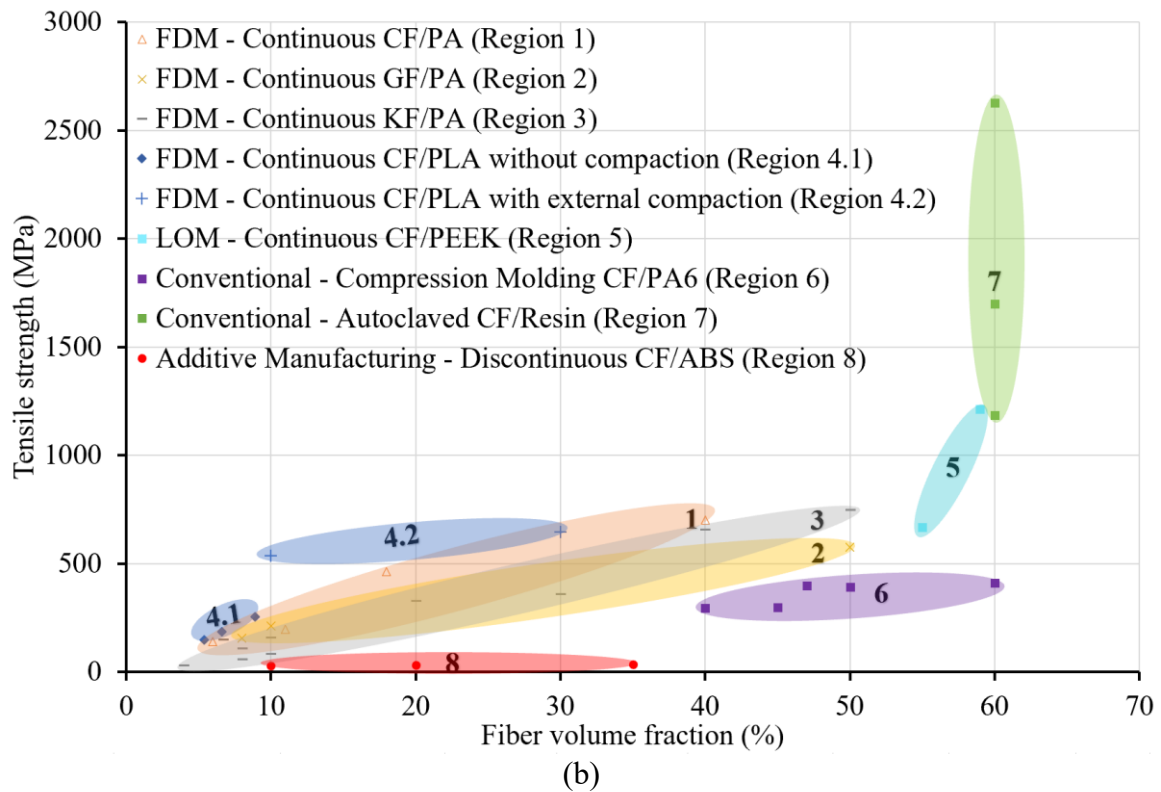
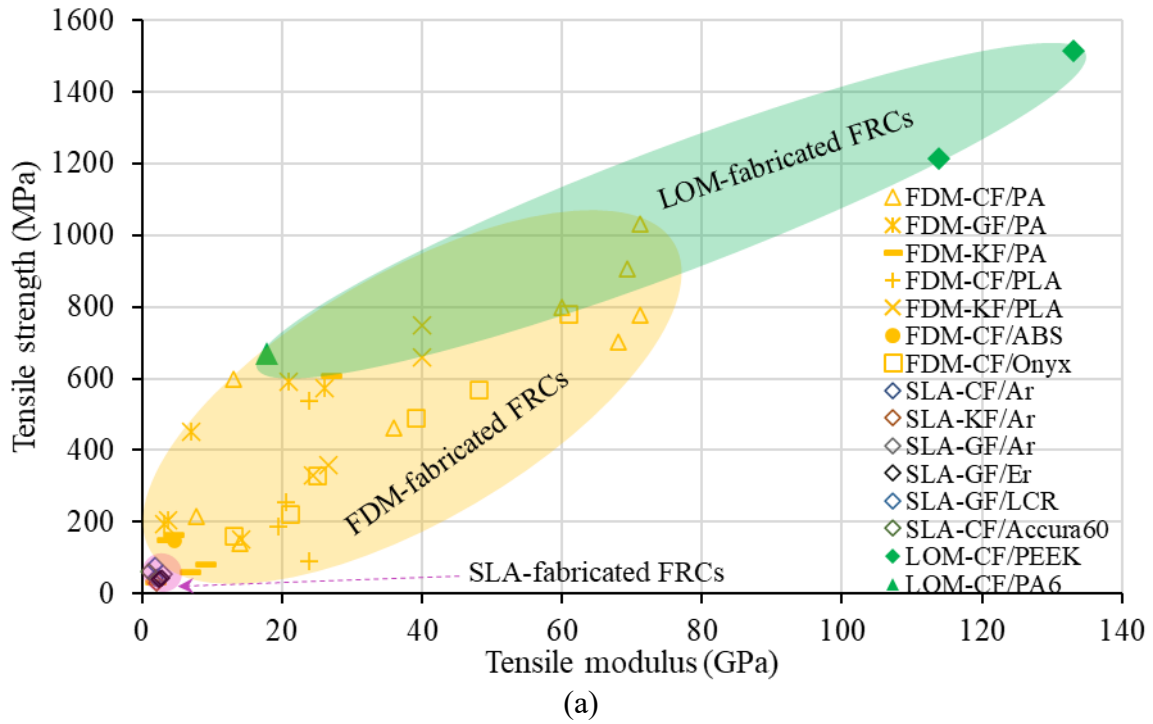


Fig. 20. (a) Tensile strength vs. tensile modulus of AM-fabricated continuous FRCs; (b) tensile strength vs. fiber volume fraction of different AM-fabricated continuous FRCs (data from [41, 77, 88-93, 96, 99, 105, 106, 108-112, 115, 130, 133, 136-141]).

4. Applications of AM-fabricated fiber reinforced composites

With nearly 10 years of concerted research, the current AM processes allow the fabrication of high-quality FRCs which can be used not only as non-structural components but also in more demanding areas such as unmanned aircrafts [142, 143] and aerospace [144, 145]. Examples of the applications of AM-fabricated FRCs are described in this section.

4.1. Tools and molds

AM offers dramatic benefits over traditional manufacturing approaches for tooling and molding in terms of cost and production time. For instance, in the automotive industry, Dunlop Systems and Components fabricated customized CF/PA tools to replace its old or broken metal tools for manufacturing electric cars [146]. Moreover, Nylon fixtures were typically used by Dunlop to hold components in place during crimping, which tended to warp at relatively high working temperature (275 °C). These fixtures have now been replaced with AM-fabricated tools made of Markforged's Onyx. Furthermore, Dunlop also AM-fabricated customized tools to manufacture a newly designed electric car to help bring the prototype into real production. The AM not only accelerates the design process of tools but is also cost-efficient.

The Big Area Additive Manufacturing (BAAM) system was first developed at Oak Ridge National Laboratory (ORNL). The material output rate is approximately 45 kg/hour and the component's final dimensions are approximately 6 m × 2.5 mm × 1.8 m [147]. A full-scale Boeing 777-X trim tool was successfully printed with the commercial BAAM system using CF/ABS at Cincinnati Incorporated© [148, 149], whose production time was reduced significantly from three months to 30 hours.

Garry Rogers Motorsport [150], an Australian motor racing team competing in both the S5000 and Australian TCR championships, recently used a Mark Two printer to successfully fabricate CF/PA brake duct mold, saving \$925 and reducing the fabrication time by 92% for





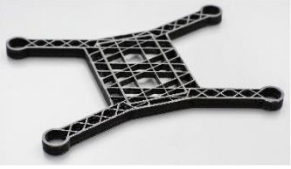
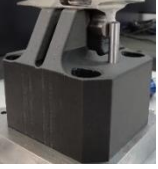


each component compared with the counterparts fabricated by traditional methods. The AM-fabricated structural components, such as brake deflector and wing spoiler, have very complex geometry and great aerodynamic characteristics. In addition, the engine parts, such as intake pipe and manifold, are made of short CF reinforced Nylon composites, which guarantees sound strength and durability while the weight is only half of the original iron parts.

4.2. End-use products

AM can also be applied to produce end-use products. For example, three Dutch companies Royal DSM, Royal Haskoning DHV, and CEAD Group collaborated to produce the first AM-fabricated FRC pedestrian footbridge (Table 4) with a dimension of 4 m × 2 m × 1.5 m by using its own continuous fiber additive manufacturing (CFAM) Prime printer, which is one of the world's largest extrusion-based 3D printer. Recyclable glass-filled thermoplastic polyester provided by DSM was employed to successfully fabricate composites with mechanical performance comparable to that of injection molded composites [151].

Haddington Dynamics [152] printed its new Dexter robotic arms (Table 4) using continuous CF reinforced composites fabricated by a Mark Two printer. The newly designed arm is almost completely made of AM-fabricated composite components, which reduces the total number of components from 800 to 70. Moreover, the total volume of materials used has been decreased and the production time has been reduced by 70%. Furthermore, since the company no longer needs to seek assistance from a third party for fabrication, the total cost of manufacturing one Dexter robotic arm has been reduced by 58%.

Table 4 Applications of AM-fabricated fiber reinforced composites

Application	Material	Materials	Industry (Company)
Footbridge [151]		Continuous GF reinforced thermoplastic (Recycled matrix material)	Infrastructure and Construction (Composite Additive Manufacturing)
Bicycle frames [153]		Continuous CF reinforced thermoplastic	Sport (Arevo)
Helicopter blades mold [154]		Carbon nanofiber reinforced PESU (Autoclave processable matrix material)	Additive Manufacturing (Thermwood)
Tools for vehicle maintenance [155]		Continuous CF reinforced Onyx	Automotive (Dayco)
Unmanned aerial vehicle [156]		Continuous CF reinforced thermoplastic with thermoset wrapping	Additive Manufacturing (Anisoprint)
Coordinate measurement machine (CMM) fixtures [157]		Discontinuous CF reinforced PA	Aerospace (JJ Churchill Ltd.)
Molds and prototypes [158]		Continuous GF reinforced Onyx	Electrical Engineering (Fischer Connectors)
Robotic arm [152]		Continuous CF reinforced PA	Artificial Intelligence (Haddington Dynamics)

5. Limitations and recommendations for future work

5.1. Feedstock materials for AM-fabricated FRCs

5.1.1 Fibers

For FDM-fabricated discontinuous FRCs, the fiber length is diverse and shorter than 400 μm due to the high-speed stirring. Therefore, such FRCs have lower mechanical properties and can only be used in non-structural components which do not require high stiffness and strength [159]. Moreover, adding fibers increases the viscosity of the filaments [160, 161] and may clog the printing nozzle [162]. One possible approach to decrease the viscosity of filaments during the fabrication process is to mix softeners with melted polymers and short fibers. Printing at a higher temperature also helps to improve the fluidity of the material [163] to prevent clogging.

On the other hand, thickeners that increase viscosity can be employed to improve stability and processability of ink in DIW and resin in SLA [164, 165].

A common issue for FDM, DIW and SLA is uneven fiber distributions and random fiber orientations in the printed components. In order to align fibers in a desired orientation, power plant and vibration could be introduced in DIW [46], and controllable magnetic field or vibration device could be employed in SLS and SLA. However, these additional operations have to be carried out by operators. Integration of such operations is expected in future commercial printers.

5.1.2 Matrix

For FDM-fabricated discontinuous FRCs, the most used matrix materials are PA, PLA and ABS. Although Polypropylene (PP), Polyethylene (PE) [166] and Polyethylene-terephthalate-glycol (PETG) [50] have been employed as the matrix for AM, there are associated problems, such as the warping and distortion of printed components [167]. Spoerk et al. [168] reported that adding expanded perlite into PP

could reduce the shrinkage and warpage of printed materials, which also promoted the adhesion between printed materials and the build platform. More efforts are expected on introducing chemical substances to fabricate matrix filaments to improve not only the printing accuracy, but also the mechanical properties of FRCs.

Both DIW and SLA utilize photosensitive thermosetting resins as matrix materials, which are limited and expensive. The liquid photosensitive resins are toxic and have odors, and the matrix materials must be stored in the dark to prevent the polymerization reaction before printing. Moreover, due to the photosensitive characteristics of the resins, the mechanical properties of the DIW and SLA-fabricated FRCs deteriorate over time if exposed to light. Furthermore, the composites fabricated by SLA and DIW are required to be cured afterward, and the post-processing is relatively complicated [169]. For DIW and SLA, more types of thermosetting resins are expected to be developed. Mixing thermosensitive resins with photosensitive resins to form resins with dual-cure possibilities could be employed. Alim et al. [170] mixed hexane dithiol (HDT), diallyl terephthalate (DAT) and trimethyl benzoyl diphenyl phosphine oxide (TPO) to form a thermoplastic-based resin that was photopolymerizable and the composites were successfully printed by SLA technique. Therefore, novel combinations of thermoplastic with photosensitive resins can broaden the possible choices of matrix materials for DIW and SLA.

For SLS-fabricated FRCs, a large variety of matrix materials can be used. Theoretically, any powder materials that can form interatomic bonds after heating can be used as matrix materials for SLS [171]. However, it is challenging for SLS to utilize matrix materials with high melting points such as PEEK or ceramics [172]. Efforts may be taken to maintain relatively high powder-bed temperature for those matrix materials that require high-processing temperature.

5.2. Printers

5.2.1 Printing logic

One common issue for desktop composite printers is that there is no sensor to monitor the printing process. If printing errors occur, such as layer misalignment, running out of filaments and/or clogged nozzles, the printing may fail eventually if the operator is not able to intervene in a timely manner. In order to save the cost of manpower monitoring and ensure the printing success rate, the printing head such as that of the latest industrial scale printer Markforged X7 can be equipped with a real-time monitoring and scanning system for closed-loop calibration. Tlegenov et al. [173] proposed a current-based sensing method for real-time monitoring of the nozzle status. When clogging is detected, the printer will stop automatically and allow an operator to correct the error so that printing can be resumed.

For FDM-fabricated discontinuous FRCs, if the printed part has an irregular shape, an inclined angle greater than 45° , or an overhanging structure, then a support is normally required. The inability to directly print an overhanging part greatly limits the fabrication of long-thin unsupported structures [174]. Removing the support usually does not cause damage to the printed part, though the interface between the support and the printed part may become very rough. In addition, the printing speed for supports is usually slower than for the actual part because the support structure is usually slender and can only be printed out successfully at a low speed. This causes the entire printing process to be both material- and time-consuming. Under normal circumstances, supports are automatically generated by the software and are not part of the STL file that is generated by the users. One possible solution could be that the users turn off the support generating function in the software and design supports independently according to their needs to reduce printing time and material consumptions. Moreover,

dual-nozzle printers may utilize one nozzle to print a support with a weaker material and another nozzle to print the actual material.

For SLA-fabricated discontinuous FRCs, the SLA process is accompanied by both physical and chemical reactions, during which the soft and thin parts may easily warp and deform, and greatly affects the overall dimensional accuracy of the printed components. Therefore, support structures are always needed no matter whether there is an overhanging part. Moreover, the removal of support materials usually requires tools such as scissors and sometimes chemical reagents, which is time-consuming and challenging [175].

For FDM-fabricated continuous FRCs, fibers can only be printed in the plane parallel to the printing platform. Therefore, the tensile properties in the out-of-plane direction (perpendicular to the printing platform) are low. Manufacturers may imitate the advanced CNC system [176] and replace the existing three-axis system with a multi-axis nozzle to be able to print fibers along the out-of-plane direction.

5.2.2 Slicing software

Discontinuous FRCs are usually printed using slicing software, either Cura or Simplify3D or self-developed program, to generate G-code and complete the printing. Users can use these slicing software packages to adjust the printing speed, nozzle temperature, platform temperature, layer thickness and infill patterns, etc. The printing accuracy, usage of materials and printing time [177] are all affected by the slicing software. Šljivic et al. [178] compared several most commonly used slicing software and concluded that Simplify 3D was the best which guaranteed better printing quality with reasonable usage of feedstock materials and printing time. On the other hand, for continuous fibers, most researchers use Markforged printers and the slicing software, Eiger, is the only compatible software. Eiger does not allow users to change operational

settings such as printing temperature (default 255 °C for fiber nozzle and 275 °C for matrix nozzle), printing speed (default 60 mm/s) and layer height (0.125 mm for CF, 0.1 mm for GF and KF), and nozzle diameter cannot be changed either. It is well known that nozzle diameter, layer thickness and printing temperature affect the mechanical performances of AM-fabricated FRCs [179, 180].

The default settings of Markforged printers ensure the consistency of the printed materials and prints, which is beneficial for industrial production. However, for scientific research, more tunable printing parameters will enable researchers to develop a deeper understanding of AM-fabricated continuous FRCs, thereby promoting the development of the entire additive manufacturing industry.

5.3. Printing quality

One notable drawback of FDM-fabricated FRCs is the relatively rough surface finishing appearances [181]. Immersing printed parts in acetone or exposing in acetone vapor have been proven to be effective to lower the roughness of finished surfaces [182, 183]. However, the use of acetone negatively affects the mechanical properties of AM-fabricated parts [184, 185].

Another intrinsic drawback of AM-fabricated FRCs is the voids in the printed materials. FRCs produced by traditional methods also have voids, but due to the high temperature and high pressure, the porosity can be controlled within 3% and thus the impact on the mechanical properties is negligible [186]. On the other hand, the porosity in printed composites is in the range of 20% to 26% [187]. Voids often appear between matrix and fiber due to the low fluidity of the melted matrix, which causes poor bonding between the fiber and matrix. A compression roller and a heated closed chamber may be installed in 3D printers to improve the bonding quality. However, this may bring in other problems, such as the addition of a compression roller may affect the moving path

of the printing head and curved shapes may not be printed smoothly. In addition, postprocessing such as annealing can also reduce the porosity and improve the mechanical properties. Several studies [188-190] found that an additional annealing process below the glass transition temperature of each material could facilitate the reflow of materials to fill the pores and gaps, hence resulted in higher mechanical properties. Rangisetty and Peel [191] reported that the tensile strengths of discontinuous CF/PLA, CF/ABS and CF/PETG increased by 16.8%, 3.3% and 12.4%, respectively, after introducing the annealing process. However, no research is published yet on the performance of continuous FRCs after annealing process and this can be explored in the near future.

Besides voids' formation, other potential issues include fiber waviness and misalignment while laying down the fibers. Manufacturers may consider adding a pre-tensioning device on the path of conveying fibers so that the fibers are always in a slight tension state.

5.4. Mechanical properties of AM-fabricated FRCs

More papers and data have been published on the mechanical properties of discontinuous FRCs than continuous FRCs. Most publications [89, 91, 96, 111, 112] with tensile modulus and strength due to the convenience of AM-fabrication of tensile coupons and conducting uniaxial tensile tests. Modulus and strength results for flexural, compressive or shear modes have been presented, though data are limited. On the other hand, materials are often subjected to dynamic or impact or cyclic loads when they are in service. However, only Charpy impact tests have been conducted to date and very few papers deal with fatigue [192, 193] and creep resistance [194, 195] of AM-fabricated FRCs. It is imperative to conduct comprehensive dynamic and fatigue tests

to understand the deformation mechanisms and load carrying capacity of AM-fabricated FRCs under various loading conditions.

5.5. Numerical simulation and theoretical prediction

Very few finite element analysis (FEA) has been reported on the mechanical performance of AM-fabricated FRCs due to the lack of proper packages available. Commercial software packages such as ANSYS or ABAQUS, which have been used to simulate composite materials and structures fabricated by traditional manufacturing techniques, are not able to capture the characteristics (such as a large portion of pores) of AM-fabricated composites. Most of simulation studies are based on topological optimization by using open-hole structures [196]. New software or numerical code is required to be developed.

Volume Averaging Stiffness (VAS) [92, 197, 198] and Rule of Mixing (ROM) [199] are the most commonly used approaches to predict the mechanical properties of AM-fabricated FRCs (both discontinuous and continuous). However, these models generally assume perfect fiber-matrix bonding and ignore voids. New constitutive or empirical models are also needed that take into account the effect of defects in bonding and voids stemmed from the AM processes.

6. Summary

This paper provides a critical review on the five additive manufacturing (AM) techniques (FDM, DIW, SLS, SLA and LOM) currently used to fabricate fiber-reinforced composites (FRCs), focusing on the mechanical properties and deformation mechanisms of AM-fabricated FRCs subjected to tension, compression, shear and flexure. The effects of feedstock materials such as fiber/matrix type and fiber weight/volume fraction, as well as processing parameters (e.g., stacking sequence and

printing temperature) on the mechanical properties of AM-fabricated FRCs have been discussed in detail. For discontinuous fiber-reinforced composites, FDM-fabricated FRCs have similar tensile strength, while higher tensile modulus than those manufactured by DIW, SLA, and SLS. It is noteworthy that modified FDM-fabricated FRCs possess both tensile modulus and strength that could compete with those manufactured by traditional injection molding. For continuous fiber-reinforced composites, LOM- and FDM-fabricated carbon fiber reinforced polyamide composites displayed superior tensile strengths which are higher than and similar to those manufactured by traditional compression molding, respectively. However, the tensile strengths of AM-fabricated FRCs are still inferior to those of the counterparts fabricated by traditional autoclave process due to the high pressure and temperature used in the traditional autoclave process.

In addition, the current limitations, e.g., limited choice of feedstock materials, relatively weak fiber/matrix bonding and high porosity, which have impeded the current wide applications of AM-fabricated FRCs, have also been presented. Possible solutions and recommendations for future work have been subsequently proposed.

Acknowledgements

The first author is grateful for the financial support through a postgraduate research scholarship from the Australian Government's Automotive Engineering Graduate Program (No. AEGP000019).

Appendix

Table A1 Summary of mechanical properties for AM-fabricated discontinuous fiber-reinforced composites (E_T : Tensile modulus, σ_T : Tensile strength, E_C : Compressive modulus, σ_C : Compressive strength, E_F : Flexural modulus, σ_F : Flexural strength, G: Shear modulus, σ_S : Shear strength, E' : Storage modulus, K_V : Charpy V-notch, ε : Strain)

Method	Materials	E_T (GPa)	σ_T (MPa)	Other properties		Refs.
				E_F (GPa)	σ_F (MPa)	
	2 wt.% CF/PA12	1.5 ± 0.13	54 ± 1.5	1.8	3	
	4 wt.% CF/PA12	2.0 ± 0.06	59 ± 3.7	2.6	71	[30]
	6 wt.% CF/PA12	2.8 ± 0.11	78 ± 2.1	4.2	96	
	8 wt.% CF/PA12	3.4 ± 0.15	88 ± 6.4	4.5	108	
	10 wt.% CF/PA12	3.6 ± 0.24	94 ± 1.4	5.3	125	
	20 wt.% CF/PA6	6.2	52	E_C (GPa) 3.9	σ_C (MPa) 56	[74]
	Onyx (CF/PA6)	2.4	40	E_F (GPa) 3.1	σ_F (MPa) 71	[77]
	Onyx (CF/PA6)	1.4	30	E_F (GPa) 2.9	σ_F (MPa) 81	[78]
	6 wt.% CF/PA	—	—	G (GPa) 0.3	σ_S (MPa) 19	[137]
	6 wt.% CF/PA6	1.9	34	E_F (GPa) 3.0	σ_F (MPa) 55	[29]
	17 wt.% CF/PA6	4.6	84	7.5	138	
FDM	12 wt.% CF/PA6 T= 200 °C HDPF	17.5 ± 2.5	250 ± 15.0	—	—	
	12 wt.% CF/PA6 T= 260 °C HPDF	17.5 ± 1.5	200 ± 5.0	—	—	
	12 wt.% CF/PLA T= 170 °C HPDF	20.5 ± 3.1	220 ± 3.0	—	—	[29]
	12 wt.% CF/PLA T= 210 °C HPDF	24.5 ± 2.5	300 ± 80	—	—	[34]
	12 wt.% CF/ABS T= 177°C HPDF	13.5 ± 2.5	90 ± 10.0	—	—	
	12 wt.% CF/ABS T= 260°C HPDF	25.0 ± 1.5	320 ± 19.1	—	—	
	20 wt.% CF/ABS (longitudinal)	11.9	66	—	—	
	20 wt.% CF/ABS (transverse)	2.1	10	—	—	[25]
	20 wt.% GF/ABS	5.7	54	—	—	
	40 wt.% GF/ABS	10.8	51	—	—	
15 wt.% CF/ABS (longitudinal)	8.9	71	—	—		
15 wt.% CF/ABS (transverse)	1.5	7	—	—	[41]	
10 wt.% CF/ABS	7.7	52	—	—		
20 wt.% CF/ABS	11.5 ± 0.5	60 ± 1.0	—	—		
30 wt.% CF/ABS	13.8	62	—	—	[26]	
40 wt.% CF/ABS	13.7	67	—	—		

Method	Materials	E_T (GPa)	σ_T (MPa)	Other properties		Refs.	
FDM	3 wt.% CF/ABS	2.1	40	—	—	[32]	
	5 wt.% CF/ABS 100 μ m fiber	1.2	39	—	—		
	5 wt.% CF/ABS 150 μ m fiber	2.4	43	E_F (GPa) 2.9	σ_F (MPa) 67		
	7.5 wt.% CF/ABS	2.5	43	—	—		
	10 wt.% CF/ABS	2.2	34	—	—		
	15 wt.% CF/ABS	2.3	36	—	—		
	5 wt.% CF/ABS T=200 °C	0.68	23	—	—		[38]
	5 wt.% CF/ABS T=210 °C	0.75	25	—	—		
	5 wt.% CF/ABS T=220 °C	0.89	32	—	—		
	5 wt.% CF/ABS T=230°C	0.68	22	—	—		[38]
	5 wt.% CF/ABS T=240°C	0.65	18	—	—		
	15 wt.% CF/ABS 0° Raster	5.9	39	—	—	[200]	
	15 wt.% CF/ABS -45°/45° Raster	2.8	29	—	—		
	15 wt.% CF/ABS 90° Raster	2.2	14	—	—		
	20 wt.% CF/ABS	8.4	67	—	—	[40]	
	4 wt.% xGnP/ABS	2.6	36	—	—	[201]	
	8 wt.% xGnP/ABS	3.5	38	—	—		
	15 wt.% CF/PLA (longitudinal)	7.5	53	—	—	[36]	
	15 wt.% CF/PLA (transverse)	3.9	35	—	—		
					E_F (GPa)	σ_F (MPa)	
	5 wt.% CF/PEEK	—	94 \pm 2.0	—	156 \pm 4.5	[31]	
	10 wt.% CF/PEEK	—	85 \pm 3.5	—	151 \pm 3.1		
	15 wt.% CF/PEEK	4.0 (calculate d)	83 \pm 1.3	—	147 \pm 2.2		
	5 wt.% GF/PEEK	—	94 \pm 3.0	—	165 \pm 3.0		
	10 wt.% GF/PEEK	—	83 \pm 3.9	—	152 \pm 4.2		
	15 wt.% GF/PEEK	—	79 \pm 2.3	—	151 \pm 1.6		
				E_F (GPa)	σ_F (MPa)		
DIW	3.5% Vf KF/EPON826	—	—	3.8	78	[48]	
	6.3% Vf KF/EPON826	—	—	4.2	108		
	B33 Photocurable (33 wt.% Ar/PA)	2.6	35	—	—	[43]	
	B50 Photocurable (50 wt.% Ar/PA)	2.7	16	—	—		

Method	Materials	E_T (GPa)	σ_T (MPa)	Other properties		Refs.
DIW	GF/B33	3.5	42	—	—	[43]
	CF/B50	3.9	31	—	—	
	CF/B50 (with sizing)	4.4	34	—	—	
	CF/PA12 - <i>x</i> direction	6.3	67	—	—	[49]
	CF/PA12 - <i>y</i> direction	3.6	54	—	—	
	CF/PA12 - <i>xy</i> direction	4.1	57	—	—	
	CF/PA12 - <i>x</i> 45°	2.4	31	—	—	
	CF/PA12 - <i>y</i> 45°	2.1	32	—	—	
	CF/PA12 - <i>xy</i> 45°	2.1	31	—	—	
					E_F (GPa)	
	30wt.% CF/PA12	—	—	2.7	76	[51]
	40wt.% CF/PA12	—	—	3.2	97	
	50wt.% CF/PA12	—	—	4.7	113	
	3 wt.% CNFs/PA12	—	—	E' (GPa)		[53]
				1.2		
SLS				E_F (GPa)	σ_F (MPa)	[202]
	30 wt.% CF/PA12	5.5	72	5.3	106	
	30 wt.% CF/PA12 HNO ₃ and heat	5.8	80	5.9	114	
	CF/PA12/Epoxy	—	101		σ_F (MPa)	[60]
					153	
	10 wt.% CF/PEEK	2.8	89	—	—	[55]
				E_F (GPa)	σ_F (MPa)	
	5 wt.% CF/PEEK	7.4	90	6.1	183	[59]
	10 wt.% CF/PEEK	7.5	109	5.2	170	
	15 wt.% CF/PEEK	7.3	70	6.1	150	
	20 wt.% CF/PEEK	6	50	4.9	80	
	10 wt.% CF/PEEK Thickness=0.1mm	7.4	109	—	—	
	10 wt.% CF/PEEK Thickness=0.15mm	5.5	50	—	—	
	10 wt.% CF/PEEK Thickness=0.2mm	4.1	40	—	—	
SLA	0.5 wt.% CNCs/SLR	3.4	74	—	—	[65]
	1 wt.% CNCs /SLR	3.6	77	—	—	
	2 wt.% CNCs /SLR	3.9	82	—	—	
	1 wt.% SiO ₂ /SLR	1.7	46	—	—	[66]
	3 wt.% SiO ₂ /SLR	2.0	50	—	—	
	5 wt.% SiO ₂ /SLR	2.7	54	—	—	
		0.1 wt.% GO/Grey resin	—	45	—	—
	0.5 wt.% GO/Grey resin	—	55	—	—	

Method	Materials	E_T (GPa)	σ_T (MPa)	Other properties		Refs.
	1 wt.% GO/Grey resin	—	60	—	—	[67]
SLA	10 wt.% GF/LCR	0.2	15	—	—	[62]
	20 wt.% GF/LCR	0.2	16	—	—	
	30 wt.% GF/LCR	0.4	17	—	—	
	40 wt.% GF/LCR	0.5	20	—	—	
	50 wt.% GF/LCR	1.0	22	—	—	
	7% Vf GF/Ar	—	27	—	—	[68]

Table A2 Summarized mechanical properties for AM-fabricated continuous fiber-reinforced composites

Method	Materials	E_T (GPa)	σ_T (MPa)	E_F (GPa)	σ_F (MPa)	Other properties		Refs.
	27% Vf CF/PA	62.5	968	41.6	485	G (GPa) 2.3	σ_S (MPa) 31	[137]
						E_C (GPa)	σ_C (MPa)	
	40% Vf CF/PA	60	800	51	540	54	320	[77]
	40% Vf GF/PA	21	590	22	200	21	140	
	40% Vf KF/PA	27	610	26	240	28	97	
	CF filaments	61.0	767	35.8	546	—	—	[203]
	CF with compression	83.2	940	57.3	1052	—	—	
	41% Vf CF/PA	13	600	38	430	—	—	[108]
	35% Vf GF/PA	7	450	15	149	—	—	
FDM	6% Vf CF/PA	14	140	—	—	—	—	[93]
	18% Vf CF/PA	36	464	—	—	—	—	
	11% Vf CF/PA	7.7	216	13.0	250	—	—	
	8% Vf GF/PA	3.1	194	3.9	166	—	—	
	10% Vf GF/PA	3.8	206	4.2	197	—	—	[89]
	8% Vf KF/PA	3.6	150	4.6	107	—	—	
	10% Vf KF/PA	4.4	164	6.7	126	—	—	
	4% Vf KF/PA	1.8	31	—	—	—	—	
	8% Vf KF/PA	6.9	60	—	—	—	—	[92]
	10% Vf KF/PA	9.0	84	—	—	—	—	
	35% Vf CF/PA	71.2	777	52	583	—	—	[110]
	35% Vf CF/PA_3DCP	71.2	1031	66	945	—	—	

Method	Materials	E_T (GPa)	σ_T (MPa)	E_F (GPa)	σ_F (MPa)	Other properties		Refs.
						E_C (GPa)	σ_C (MPa)	
	41% Vf CF/PA	68	701	—	—	53	223	[90]
	50% Vf GF/PA	26	575	—	—	20	82	
						E_C (GPa)	σ_C (MPa)	
	8.18% Vf CF/PA	—	—	—	—	1.5	40	
	16.59% Vf CF/PA	—	—	—	—	1.9	43	
	17.18% Vf CF/PA	—	—	5.2	84	—	—	[106]
	24.44% Vf CF/PA	—	—	—	—	2.1	53	
	32.19% Vf CF/PA	—	—	8.9	143	—	—	
	48.93% Vf CF/PA	—	—	14.2	231	—	—	
						σ_S (MPa)		
FDM	27.2% Vf CF/PA	—	—	—	—	22.2		
	27.2% Vf GF/PA	—	—	—	—	13.9		
	27.2% Vf KF/PA	—	—	—	—	13.7		[107]
	73.2% Vf CF/PA	—	—	—	—	31.9		
	73.2% Vf GF/PA	—	—	—	—	21.0		
	73.2% Vf KF/PA	—	—	—	—	14.3		
						K_V (kJ/m ²)		
	24.9% Vf CF/PA	—	—	—	—	33		[97]
	29.2% Vf GF/PA	—	—	—	—	207		
	29.5% Vf KF/PA	—	—	—	—	84		
						E_C (GPa)	σ_C (MPa)	
	31.4% Vf CF/PA	69.4	905	—	—	63.9	426	[109]
						K_V (kJ/m ²)		
	CF/PEEK	—	—	37	480	56		[98]

Method	Materials	E_T (GPa)	σ_T (MPa)	E_F (GPa)	σ_F (MPa)	Other properties	Refs.
	10 wt% or 8.9% Vf	20.6	256	14.5	220	K_V (kJ/m ²) 35 for original CF/PLA	[99]
	10 wt% or 8.9% Vf CF/PLA (Recycled)	20.6	260	13.3	263	39 for recycled CF/PLA	
	25% CF/PLA	—	—	30	335	—	[101]
	6.6% Vf CF/PLA	19.5	185	—	—	—	[88]
	6.1% Vf Jute/PLA	5.1	57	—	—	—	
	34% Vf CF/PLA	23.8 (calculated)	80	—	59	—	[91]
	34% Vf CF/PLA With sizing	—	91	—	156	—	
	8.6% Vf AF/PLA	9.3	203	—	—	—	[136]
	6.7% Vf AF/PLA	14.2	150	—	—	—	
FDM	20% Vf AF/PLA	24.5	330	—	—	—	
	30% Vf AF/PLA	26.6	360	—	—	—	[105]
	40% Vf AF/PLA	40.0	660	—	—	—	
	50% Vf AF/PLA	40.0	750	—	—	—	
	30% Vf CF/PLA	49.1	393	25.1	157	—	
	30% Vf CF/PLA With compaction	63.9	536	24.0	222	—	[115]
	10% Vf CF/PLA	—	110	—	163	—	
	10% Vf CF/PLA With compaction	—	645	—	401	—	[125]
	10 wt% CF/ABS	4.2	147	—	127	—	[94]
	15.16% Vf CF/Onyx	13	160	—	—	—	
	30.10% Vf CF/Onyx	25	330	—	—	—	[96]
	47.50% Vf CF/Onyx	39	490	—	—	—	

Method	Materials	E_T (GPa)	σ_T (MPa)	E_F (GPa)	σ_F (MPa)	Other properties		Ref.
FDM	71.33% Vf CF/Onyx	48	570	—	—	—	—	[96]
	15% Vf CF/Onyx	21.1	224	—	—	—	—	[112]
	27% Vf CF/Onyx	60.9	780	—	—	—	—	[111]
	38.27 wt.% CF/PEEK	—	—	37	480	—	—	[98]
	54.8 wt.% GF/PP	—	—	13	—	—	—	[113]
SLA	7 gm ⁻² CF/Ar	1.8	44	—	—	—	—	[127]
	17 gm ⁻² CF/Ar	2.5	42	—	—	—	—	
	17 gm ⁻² KF/Ar	2.1	30	—	—	—	—	
	7 gm ⁻² GF/Ar	2.2	44	—	—	—	—	
	17 gm ⁻² GF/Ar	2.9	55	—	—	—	—	
	34 gm ⁻² GF/Er	2.8	42	—	—	—	—	
	50 gm ⁻² GF/Er	2.4	39	—	—	—	—	
	GF/LCR	1.8	79	—	—	—	—	[62]
CF/Accura60 resin	1.0	60	—	—	—	—	[126]	
LOM	59% Vf CF/PEEK Without hot-press	113.8	1213	89.7	671	—	—	[130]
	59% Vf CF/PEEK With hot-press	133.1	1514	125.7	1901	—	—	
	49% Vf CF/PA6 With ultrasound	105.7 ± 7.2	1760 ± 71.7	96.5 ± 5.1	1026 ± 52.3	—	—	[131]
	55% Vf CF/PA6	18.0	668	—	591	—	—	[134]
	52%-55% Vf GF/Epoxy	—	713	—	1190	—	σ_C (MPa) 896	[133]

Table A3 Summary of mechanical properties of traditionally fabricated discontinuous fiber reinforced composites

<i>Method</i>	<i>Material</i>	E_T (GPa)	σ_T (MPa)	ε (At break)	<i>Ref.</i>
<i>Injection molding</i>	21 Vf% Short CF/PA66	13	124	1.68%	[75]
	31 Vf% Short CF/PA66	22	150	1.26%	
	20 Vf% Long CF/PA66	23	158	0.97%	
	32 Vf% Long CF/PA66	29	173	0.78%	

Table A4 Summary of mechanical properties of traditionally fabricated continuous fiber reinforced composites

<i>Method</i>	<i>Material</i>	E_T (GPa)	σ_T (MPa)	σ_c (MPa)	<i>Refs.</i>
<i>Compression Molding</i>	40% Vf	28.3	296	271	[138]
	50% Vf	48.1	393	323	
	60% Vf	50.2	410	367	
	78% Vf	-	768	418	[140]

References

- [1] I. Campbell, D. Bourell, I. Gibson, *Rapid Prototyp. J.* 18 (2012) 255-258.
- [2] Y. Li, Y. Lou, *Polymers* 12 (2020) 2497.
- [3] P. Parandoush, D. Lin, *Compos. Struct.* 182 (2017) 36-53.
- [4] N. van de Werken, H. Tekinalp, P. Khanbolouki, S. Ozcan, A. Williams, M. Tehrani, *Addit. Manuf.* 31 (2020) 100962.
- [5] B. Brenken, E. Barocio, A. Favaloro, V. Kunc, R.B. Pipes, *Addit. Manuf.*, 21 (2018) 1-16.
- [6] S.M.F. Kabir, K. Mathur, A.F.M. Seyam, *Compos. Struct.* 232 (2020) 111476.
- [7] W. Sachini, D. Truong, T. Phuong, *Polymer*, 12 (2020) 12071529.
- [8] A. Le Duigou, D. Correa, M. Ueda, R. Matsuzaki, M. Castro, *Mater. Des.*, 194 (2020) 108-911.
- [9] J. Šafka, M. Ackermann, J. Bobek, M. Seidl, J. Habr, L. Běhálek, *Mater. Sci. Forum* 862 (2016) 174-181.
- [10] N.E. Zander, J.H. Park, Z.R. Boelter, M.A. Gillan, *ACS Omega* 4 (2019) 13879-13888.
- [11] A. El Magri, K. El Mabrouk, S. Vaudreuil, M. Ebn. Touhami, *J. Thermoplast. Compos. Mater.* 34 (2021) 581-595.
- [12] L. Lin, N. Ecke, M. Huang, X.Q. Pei, A.K. Schlarb, *Composites, Part B* 177 (2019), 107428.
- [13] E. Yasa, in: *Proceedings of the 29th Annual International Solid Freeform Fabrication Symposium, Texas, U.S., July 25-27, 2020.*
- [14] G.D. Goh, Y.L. Yap, S. Agarwala, W.Y. Yeong, *Adv. Mater. Technol.* 4 (2018) 1800271.
- [15] A.R. Torrado Perez, D.A. Roberson, R.B. Wicker, *J. Fail. Anal. Prev.* 14 (2014) 343-353.
- [16] D. Stoof and K. Pickering, *Compos. Pt. B-Eng.* 135 (2018) 110-118.
- [17] F. Gardea, D.P. Cole, B. Glaz, J.C. Riddick, *Rapid Prototyp. J.* 26 (2019) 509-517.
- [18] M.L. Shofner, K. Lozano, F.J. Rodríguez-Macías, E.V. Barrera, *J. Appl. Polym. Sci.* 89 (2003) 3081-3090.
- [19] J. Zhu and B. Wang, *Mater. Sci. Forum* 898 (2017) 2384-2391.
- [20] K. Kinga, Ł. Michał, C. Shih-Yu, L. Wei-Ting, C. An, H.-K. Maria, G. Szymon, M. Janusz, *Materials* 13 (2020) 579.
- [21] K. Qian, X. Qian, Y. Chen, M. Zhou, *J. Appl. Polym. Sci.* 135 (2018) 46483.
- [22] I. Durgun and R. Ertan, *Rapid Prototyp. J.* 20 (2014) 228-235.
- [23] Z.C. Kennedy and J.F. Christ, *Addit. Manuf.* 36 (2020) 101233.
- [24] I. Gibson, D. Rosen, B. Stucker, *Additive Manufacturing Technologies – Rapid Prototyping to Direct Digital Manufacturing*, Springer, Boston, 2010.

- [25] C.E. Duty, T. Drye, A. Franc, Material Development for Tooling Applications Using Big Area Additive Manufacturing (BAAM), Oak Ridge, U. S., 2015.
- [26] H.L. Tekinalp, V. Kunc, G.M. Velez-Garcia, C.E. Duty, L.J. Love, A.K. Naskar, C.A. Blue, S. Ozcan, *Compos. Sci. Technol.* 105 (2014) 144-150.
- [27] S.H. Han, H.J. Oh, S.S. Kim, *Compos. Pt. B-Eng.* 60 (2014) 98-105.
- [28] S. Berretta, R. Davies, Y.T. Shyng, Y. Wang, O. Ghita, *Polym. Test.* 63 (2017) 251-262.
- [29] L.G. Blok, H. Yu, M.L. Longana, B.K.S. Woods, in: Proceedings of the 18th European Conference on Composite Materials, Athens, Greece, June 24-28, 2018.
- [30] G. Liao, Z. Li, Y. Cheng, D. Xu, D. Zhu, S. Jiang, J. Guo, X. Chen, G. Xu, Y. Zhu, *Mater. Des.* 139 (2018) 283-292.
- [31] P. Wang, B. Zou, S. Ding, C. Huang, Z. Shi, Y. Ma, P. Yao, *Compos. Pt. B-Eng.* 198 (2020), 108175.
- [32] F. Ning, W. Cong, J. Qiu, J. Wei, S. Wang, *Compos. Pt. B-Eng.* 80 (2015) 369-378.
- [33] T. Hofstätter, I. Gutmann, T. Koch, D. Pedersen, G. Tosello, G. Heinz, H. Hansen, in: Proceedings of the ASPE Summer Topical Meeting, Raleigh, U. S., July 11-13, 2016.
- [34] H. Yu, K.D. Potter, M.R. Wisnom, *Compos. Pt. A-Appl. Sci. Manuf.* 65 (2014) 175-185.
- [35] I. Ferreira, M. Machado, F. Alves, A. Torres Marques, *Rapid Prototyp. J.* 25 (2019) 972-988.
- [36] R.T.L. Ferreira, I.C. Amatte, T.A. Dutra, D. Bürger, *Compos. Pt. B-Eng.* 124 (2017) 88-100.
- [37] M. Behzadnasab and A. Yousefi, in: Proceedings of the 12th International Seminar on Polymer Science and Technology, Tehran, Iran, November 2-5, 2016.
- [38] F. Ning, W. Cong, Y. Hu, H. Wang, *J. Compos. Mater.* 51 (2017) 451-462.
- [39] Christine, Comparison of Carbon Fiber, Kevlar® (Aramid) and E Glass used in Composites for Boatbuilding, <https://www.christinedemerchant.com/carbon-kevlar-glass-comparison.html>, May 7, 2021.
- [40] C. Hill, K. Rowe, R. Bedsole, J. Earle, V. Kunc, Society for the Advancement of Material and Process Engineering, Long beach, U. S., May 23-26, 2016.
- [41] L. Love, V. Kunc, O. Ríos, C. Duty, A. Elliott, B. Post, R.J. Smith, C. Blue, *J. Mater. Res.* 29 (2014) 1893-1898.
- [42] G. Postiglione, G. Natale, G. Griffini, M. Levi, S. Turri, *Compos. Pt. A-Appl. Sci. Manuf.* 76 (2015) 110-114.
- [43] M. Invernizzi, G. Natale, M. Levi, S. Turri, G. Griffini, *Materials.* 9 (2016) 583.

- [44] G. Griffini, M. Invernizzi, M. Levi, G. Natale, G. Postiglione, S. Turri, *Polymer* 91 (2016) 174-179.
- [45] R.L. Truby and J.A. Lewis, *Nature* 540 (2016) 371-378.
- [46] B.G. Compton and J.A. Lewis, *Adv. Mater.* 26 (2014) 5930-5935.
- [47] T. George, A.K. Dutta, M.S. Islam, J.J. Martin, A. Caunter, A. Dendulk, S. Goodrich, R. Pembroke, D. Shores, R.M. Erb, *Micro- and Nanotechnology Sensors, Systems, and Applications IX*, Bellingham, U. S., April 9-13, 2017.
- [48] N. Nawafleh, F.K.E. Elibol, M. Aljaghtham, E. Oflaz, A.J. Ciciriello, C.M. Dumont, E. Dauer, R.M. Gorguluarslan, T. Demir, E. Celik, *J. Mater. Sci.* 55 (2020) 11284-11295.
- [49] A. Jansson and L. Pejryd, *Addit. Manuf.* 9 (2016) 7-13.
- [50] D. Jiang and D.E. Smith, *Addit. Manuf.* 18 (2017) 84-94.
- [51] C. Yan, L. Hao, L. Xu, Y. Shi, *Compos. Sci. Technol.* 71 (2011) 1834-1841.
- [52] G.V. Salmoria, J.L. Leite, L.F. Vieira, A.T.N. Pires, C.R.M. Roesler, *Polym. Test.* 31 (2012) 411-416.
- [53] R.D. Goodridge, M.L. Shofner, R.J.M. Hague, M. McClelland, M.R. Schlea, R.B. Johnson, C.J. Tuck, *Polym. Test.* 30 (2011) 94-100.
- [54] P. Peyre, Y. Rouchausse, D. Defauchy, G. Régnier, *J. Mater. Process. Technol.* 225 (2015) 326-336.
- [55] T.J. Hoskins, K.D. Dearn, S.N. Kukureka, *Polym. Test.* 70 (2018) 511-519.
- [56] B. Chen, S. Berretta, K. Evans, K. Smith, O. Ghita, *Appl. Surf. Sci.* 428 (2018) 1018-1028.
- [57] B. Chen, Y. Wang, S. Berretta, O. Ghita, *J. Mater. Sci.* 52 (2017) 6004-6019.
- [58] Y. Wang, D. Rouholamin, R. Davies, O.R. Ghita, *Mater. Des.* 88 (2015) 1310-1320.
- [59] M. Yan, X. Tian, G. Peng, D. Li, X. Zhang, *Compos. Sci. Technol.* 165 (2018) 140-147.
- [60] W. Zhu, C. Yan, Y. Shi, S. Wen, J. Liu, Q. Wei, Y. Shi, *Sci. Rep.* 6 (2016) 33780.
- [61] T. Rayna and L. Striukova, *Technol. Forecast. Soc. Change* 102 (2016) 214-224.
- [62] Y. Sano, R. Matsuzaki, M. Ueda, A. Todoroki, Y. Hirano, *Addit. Manuf.* 24 (2018) 521-527.
- [63] S. Zakeri, M. Vippola, E. Levänen, *Addit. Manuf.* 35 (2020) 101177.
- [64] S. Baumgartner, R. Gmeiner, J.A. Schönherr, J. Stampfl, *Mater. Sci. Eng. C* 116 (2020) 111-180.
- [65] S. Kumar, M. Hofmann, B. Steinmann, E.J. Foster, C. Weder, *ACS Appl. Mater. Interfaces.* 4 (2012) 5399-5407.
- [66] Z. Weng, Y. Zhou, W. Lin, T. Senthil, L. Wu, *Compos. Pt. A-Appl. Sci. Manuf.* 88 (2016) 234-242.

- [67] J.Z. Manapat, J.D. Mangadlao, B.D.B. Tiu, G.C. Tritchler, R.C. Advincula, *ACS Appl. Mater. Interf.* 9 (2017) 10085-10093.
- [68] A. Ogale, T. Renault, R. Dooley, A. Bagchi, C. Jara-almonte, *SAMPE J.* 23 (1991) 28-38.
- [69] P.W. Huang, H.S. Peng, S.J. Hwang, C.T. Huang, P.C. Chen, Y.Y. Ke, P.S. Pan, C.C. Wu, C.I. Tu, 77th Annual Technical Conference of the Society of Plastics Engineers, Detroit, U.S., March 18-21, 2019.
- [70] A.L.N. Inácio, R.C. Nonato, B.C. Bonse, *Polym. Test.* 72 (2018) 357-363.
- [71] Y.P. Zhang, C.G. Zhou, W.J. Sun, T. Wang, L.C. Jia, D.X. Yan, Z.M. Li, *Compos. Sci. Technol.* 197 (2020) 108253.
- [72] K. Enomoto, *New Diamond Front. Carbon Technol.* 15 (2005) 59-72.
- [73] M.P. Kujawski, ASME 2006 International Mechanical Engineering Congress and Exposition, Chicago, U. S., November 5-10, 2006.
- [74] E. Verdejo de Toro, J. Coello Sobrino, A. Martínez Martínez, V. Miguel Eguía, J. Ayllón Pérez, *Materials* 13 (2020) 672.
- [75] A. Hassan, P.R. Hornsby, M.J. Folkes, *Polym. Test.* 22 (2003) 185-189.
- [76] EOS, EOS Material Data Center, <<https://eos.materialdatacenter.com/eo/standard/main/table>>, May 9, 2021.
- [77] Markforged, Material data sheet, composites, https://static.markforged.com/markforged_composites_datasheet.pdf, October 8, 2021.
- [78] F. Bárník, M. Vaško, M. Handrik, F. Dorčiak, J. Majko, *Transp. Res. Proc.* 40 (2019) 616-622.
- [79] T.D. Ngo, A. Kashani, G. Imbalzano, K.T.Q. Nguyen, D. Hui, *Compos. Pt. B-Eng.* 143 (2018) 172-196.
- [80] A. Gupta and A.A. Ogale, *Polym. Compos.* 23 (2002) 1162-1170.
- [81] D. Karalekas and K. Antoniou, *J. Mater. Process. Technol.* 153 (2004) 526-530.
- [82] S.H. Huang, P. Liu, A. Mokasdar, L. Hou, *Int. J. Adv. Manuf. Technol.* 67 (2013) 1191-1203.
- [83] N. Travitzky, A. Bonet, B. Dermeik, T. Fey, I. Filbert-Demut, L. Schlier, T. Schlördt, P. Greil, *Adv. Eng. Mater.* 16 (2014) 729-754.
- [84] F.N. Chaudhry, S.I. Butt, A. Mubashar, A.B. Naveed, S.H. Imran, Z. Faping, *J. Thermoplast. Compos. Mater.* (2019) 352-374.
- [85] M. Heidari-Rarani, M. Rafiee-Afarani, A.M. Zahedi, *Compos. Pt. B-Eng.* 175 (2019) 107147.
- [86] Q. Hu, Y. Duan, H. Zhang, D. Liu, B. Yan, F. Peng, *J. Mater. Sci. Lett.* 53 (2018) 1887-1898.
- [87] Y. Nakagawa, K.-i. Mori, T. Maeno, *Int. J. Adv. Manuf. Technol.* 91 (2017) 2811.

- [88] M. Ryosuke, U. Masahito, N. Masaki, J. Tae-Kun, A. Hirosuke, H. Keisuke, N. Taishi, T. Akira, H. Yoshiyasu, *Sci. Rep.* 6 (2016) 23058.
- [89] A.N. Dickson, J.N. Barry, K.A. McDonnell, D.P. Dowling, *Addit. Manuf.* 16 (2017) 146-152.
- [90] J. Justo, L. Távara, L. García-Guzmán, F. París, *Compos. Struct.* 185 (2018) 537-548.
- [91] N. Li, Y. Li, S. Liu, *J. Mater. Process. Technol.* 238 (2016) 218-225.
- [92] G.W. Melenka, B.K.O. Cheung, J.S. Schofield, M.R. Dawson, J.P. Carey, *Compos. Struct.* 153 (2016) 866-875.
- [93] F. van der Klift, Y. Koga, A. Todoroki, M. Ueda, Y. Hirano, R. Matsuzaki, *J. Compos. Mater.* 6 (2016) 18-27.
- [94] C. Yang, X. Tian, T. Liu, Y. Cao, D. Li, *Rapid Prototyp. J.* 23 (2017) 209-215.
- [95] H. Mei, Z. Ali, Y. Yan, I. Ali, L. Cheng, *Addit. Manuf.* 27 (2019) 150-158.
- [96] Y. Peng, Y. Wu, K. Wang, G. Gao, S. Ahzi, *Compos. Struct.* 207 (2019) 232-239.
- [97] M.A. Caminero, J.M. Chacón, I. García-Moreno, G.P. Rodríguez, *Compos. Pt. B-Eng.* 148 (2018) 93-103.
- [98] M. Luo, X. Tian, J. Shang, W. Zhu, D. Li, Y. Qin, *Compos. Pt. A-Appl. Sci. Manuf.* 121 (2019) 130-138.
- [99] X. Tian, T. Liu, Q. Wang, A. Dilmurat, D. Li, G. Ziegmann, *J. Cleaner Prod.* 142 (2017) 1609-1618.
- [100] A.D. Pertuz, S. Díaz-Cardona, O.A. González-Estrada, *Int. J. Fatigue* 130 (2020) 105275.
- [101] X. Tian, T. Liu, C. Yang, Q. Wang, D. Li, *Composites* 88 (2016) 198-205.
- [102] T. Liu, X. Tian, M. Zhang, D. Abliz, D. Li, G. Ziegmann, *Compos. Pt. A-Appl. Sci. Manuf.* 114 (2018) 368-376.
- [103] M.A. Montes-Morán, A. Martínez-Alonso, J.M.D. Tascón, M.C. Paiva, C.A. Bernardo, *Carbon* 39 (2001) 1057-1068.
- [104] J. Li, *Appl. Surf. Sci.* 255 (2008) 2822-2824.
- [105] Z. Hou, X. Tian, Z. Zheng, J. Zhang, L. Zhe, D. Li, A.V. Malakhov, A.N. Polilov, *Compos. Pt. B-Eng.* 189 (2020) 107893.
- [106] M. Araya-Calvo, I. López-Gómez, N. Chamberlain-Simon, J.L. León-Salazar, T. Guillén-Girón, J.S. Corrales-Cordero, O. Sánchez-Brenes, *Addit. Manuf.* 22 (2018) 157-164.
- [107] M.A. Caminero, J.M. Chacón, I. García-Moreno, J.M. Reverte, *Polym. Test.* 68 (2018) 415-423.
- [108] G.D. Goh, V. Dikshit, A.P. Nagalingam, G.L. Goh, S. Agarwala, S.L. Sing, J. Wei, W.Y. Yeong, *Mater. Des.* 137 (2018) 79-89.

- [109] M. Iragi, C. Pascual-González, A. Esnaola, C.S. Lopes, L. Aretxabaleta, *Addit. Manuf.* 30 (2019) 100884.
- [110] M. Ueda, S. Kishimoto, M. Yamawaki, R. Matsuzaki, A. Todoroki, Y. Hirano, A. Le Duigou, *Compos. Pt. A-Appl. Sci. Manuf.* 137 (2020) 105985.
- [111] M. Iragi, C. Pascual-Gonzalez, A. Esnaola, J. Aurrekoetxea, C.S. Lope, L. Aretxabaleta, in: *Proceedings of the 18th European Conference on Composite Materials*, Athens, Greece, June 24-28, 2018.
- [112] Z. Lash, J. Servey, F. Gardone, C. Nikhare, S.H.R. Sanei, in: *Proceedings of the ASME 2019 International Mechanical Engineering Congress and Exposition*, Salt Lake City, U. S., Nov 8-14, 2019.
- [113] T. Vaneker, *Procedia CIRP* 60 (2017) 181-186.
- [114] Markforged, Celebrating the Last Five Years, <https://markforged.com/resources/blog/celebrating-five-years>, March 8, 2021.
- [115] R. Omuro, M. Ueda, R. Matsuzaki, A. Todoroki, Y. Hirano, in: *Proceedings of the 21st International Conference on Composite Materials*, Xi'an, China, May 15-17, 2017.
- [116] M. Rismalia, S.C. Hidajat, I.G.R. Permana, B. Hadisujoto, M. Muslimin, F. Triawan, *J. Phys. Conf. Ser.* 1402 (2019) 044041.
- [117] F. Fernandez, W.S. Compel, J.P. Lewicki, D.A. Tortorelli, *Comput. Methods Appl. Mech. Eng.* (2019) 277-307.
- [118] K. Dong, L. Liu, X. Huang, X. Xiao, *Compos. Struct.* 250 (2020) 112610.
- [119] L. Yang, R. Mertens, M. Ferrucci, C. Yan, Y. Shi, S. Yang, *Mater. Des.* 162 (2019) 394-404.
- [120] G.D. Goh, W. Toh, Y.L. Yap, T.Y. Ng, W.Y. Yeong, *Compos. Pt. B-Eng.* 216 (2021) 108840.
- [121] H. Mei, Z. Ali, I. Ali, L. Cheng, *Adv. Compos. Mater.* 2 (2019) 312-319.
- [122] H. Brooks, D. Tyas, S. Molony, *Int. J. Rapid Manuf.* 6 (2017) 97-113.
- [123] B. Huang and S. Singamneni, *J. Compos. Mater.* 49 (2015) 363-383.
- [124] A. Todoroki, T. Oasada, Y. Mizutani, Y. Suzuki, M. Ueda, R. Matsuzaki, Y. Hirano, *Adv. Compos. Mater.* 29 (2020) 147-162.
- [125] J. Zhang, Z. Zhou, F. Zhang, Y. Tan, Y. Tu, B. Yang, *Materials* 13 (2020) 471.
- [126] Y. Lu, P. Gin Kit, G. Andrew, L. Zhao, X. Han, *Proceedings of the 16th Conference on Rapid Design, Prototyping & Manufacturing*, Uxbridge, U.K., April 4-5, 2019.
- [127] D.E. Karalekas, *Mater. Des.* 24 (2003) 665-670.
- [128] F. Saffar, C. Sonnenfeld, P. Beauchene, C.H. Park, *Front. Mater.* 7 (2020) 1-12.
- [129] J.P. Davim and P. Reis, *Mater. Des.* 24 (2003) 315-324.

- [130] B. Chang, X. Li, P. Parandoush, S. Ruan, C. Shen, D. Lin, *Polym. Test.* 88 (2020), Article 106563.
- [131] B. Chang, P. Parandoush, X. Li, S. Ruan, C. Shen, R.A. Behnagh, Y. Liu, D. Lin, *Polym. Compos.* 41 (2020) 4706-4715.
- [132] S. Sommacal, A. Matschinski, K. Drechsler, P. Compston, *Composites* 149 (2021), Article 106487.
- [133] D. Klosterman, R. Chartoff, G. Graves, N. Osborne, B. Priore, *Compos. Pt. A-Appl. Sci. Manuf.* 29 (1998) 1165-1174.
- [134] P. Parandoush, C. Zhou, D. Lin, *Adv. Eng. Mater.* 21 (2019) 1800622.
- [135] F. Ahmed, S.C. Joshi, Y.C. Lam, *J. Thermoplast. Compos. Mater.*, 17 (2004) 447-462.
- [136] P. Bettini, G. Alitta, G. Sala, L. Landro, *J. Mater. Eng. Perform.* 26 (2017) 843-848.
- [137] L.G. Blok, M.L. Longana, H. Yu, B.K.S. Woods, *Addit. Manuf.* 22 (2018) 176-186.
- [138] E.C. Botelho, Ł. Figiel, M.C. Rezende, B. Lauke, *Compos. Sci. Technol.* 63 (2003) 1843-1855.
- [139] N.G. Karsli and A. Aytac, *Compos. Pt. B-Eng.* 51 (2013) 270-275.
- [140] Z. Sun, J. Xiao, L. Tao, Y. Wei, S. Wang, H. Zhang, S. Zhu, M. Yu, *Materials* 12 (2018) 13.
- [141] S.Y. Park, C.H. Choi, W.J. Choi, S.S. Hwang, *Appl. Compos. Mater.* 26 (2019) 187-204.
- [142] G.D. Goh, S. Agarwala, G.L. Goh, V. Dikshit, S.L. Sing, W.Y. Yeong, *Aerosp. Sci. Technol.* 63 (2017) 140-151.
- [143] S.K. Moon, Y.E. Tan, J. Hwang, Y.-J. Yoon, *Int. J. Precis Eng Manuf-Green Technol.* 1 (2015) 223-228.
- [144] F. Froes and R. Boyer, *Additive Manufacturing for the Aerospace Industry*, Elsevier, Cambridge, 2019.
- [145] C. Jones, E.H. Robertson, M. Koelbl, C. Singer, NASA Center for AeroSpace Information, Huntsville, U. S., May 2-6, 2018.
- [146] D. Sam, Dunlop Systems integrates Markforged 3D printing for internal and customer tooling, 3D Printing & Additive Manufacturing Intelligence, <https://www.tctmagazine.com/additive-manufacturing-3d-printing-news/dunlop-systems-markforged-3d-printing-tooling/>, October 8, 2021.
- [147] A.A. Hassen, R. Springfield, J. Lindahl, B. Post, L. Love, C. Duty, U. Vaidya, R. Pipes, V. Kunc, in: *Proceedings of the Composites and Advanced Materials Expo*, Anaheim, U. S., September 26-29, 2016.

- [148] Cincinnati, Boeing 777x Trim Tool, <https://www.e-ci.com/boeing-777x-trim-tool>, May 9, 2021.
- [149] T. Wohlers, I. Campbell, O. Diegel, J. Kowen, N. Mostow, Wohlers Report 2021-3D Printing and Additive Manufacturing, OakRidge, U. S., 2021.
- [150] Solidprint, Discover how the oldest racing team in Australia reached new levels of speed through their use of 3D printing, <https://www.solidprint3d.co.uk/success-story-garry-rogers-motorsport/>, August 10, 2021.
- [151] CEAD, CFAM Prime-Dedicated production system with thermoplastic composite materials, accessed, <https://cead-am.com/>, February 27, 2021.
- [152] Haddington Dynamics, Haddington Dynamics' latest and greatest 7+ axis robotic arm, <https://www.hdrobotic.com/dexter>, October 8, 2021.
- [153] P. Joris, AREVO Partners With Franco Bicycles to Make 3D Printed Carbon Fiber Frames, <https://3dprint.com/240923/arevo-partners-with-franco-bicycles-to-make-3d-printed-carbon-fiber-frames/>, October 8, 2021.
- [154] Thermwood, Large Scale Additive Manufacturing, http://www.thermwood.com/lam_home.htm, August 10, 2021.
- [155] C. Schwaar, Markforged X7 Case Study: 3D Printing Stronger Material, <https://all3dp.com/4/markforged-x7-case-study-3d-printing-stronger-material/>, February 26, 2021.
- [156] A. Azarov, F. Antonov, M. Golubev, A. Khaziev, S. Ushanov, Compos. Pt. B-Eng. 169 (2019) 157-163.
- [157] Markforged, JJ Churchill: CMM Inspection Fixture, <https://markforged.com/resources/application-spotlights/cmm-fixture>, October 8, 2021.
- [158] Markforged, Digital Forge for electronics manufacturing, <https://markforged.com/industries/electronics>, October 8, 2021.
- [159] Y. Kim and O.O. Park, Macromol. Res. 28 (2020) 433-444.
- [160] K.P.M. Lee, M. Brandt, R. Shanks, F. Daver, Polymers 12 (2020) 2014.
- [161] Z. Jiang, B. Diggle, M.L. Tan, J. Viktorova, C.W. Bennett, L.A. Connal, Adv. Sci. 7 (2020) 2001379.
- [162] V. Mirón, S. Ferrándiz, D. Juárez, A. Mengual, Procedia Manuf. 13 (2017) 888-894.
- [163] B. Shaqour, M. Abuabiah, S. Abdel-Fattah, A. Juaidi, R. Abdallah, W. Abuzaina, M. Qarout, B. Verleije, P. Cos, Int. J. Adv. Manuf. Technol. 114 (2021) 1279-1291.
- [164] S.A. Ntim, O. Sae-Khow, C. Desai, F.A. Witzmann, S. Mitra, J. Environ. Monit. 14 (2012) 2772-9.

- [165] S.W. Tam, R. W, S. Rashidi, A. Luqman Chuah, M. Khalid, *Int. J. Eng. Sci. Technol.* 11 (2016) 1-15.
- [166] P. Olesik, M. Godzierz, M. Koziół, *Materials* 12 (2019) 162520.
- [167] O.S. Carneiro, A.F. Silva, R. Gomes, *Mater. Des.* 83 (2015) 768-776.
- [168] M. Spoerk, J. Sapkota, G. Weingrill, T. Fischinger, F. Arbeiter, C. Holzer, *Macromol. Mater. Eng.* 302 (2017).
- [169] S. Zhang, M. Li, N. Hao, A.J. Ragauskas, *ACS Omega* 4 (2019) 20197-20204.
- [170] M.D. Alim, K.K. Childress, N.J. Baugh, A.M. Martinez, A. Davenport, B.D. Fairbanks, M.K. McBride, B.T. Worrell, J.W. Stansbury, R.R. McLeod, C.N. Bowman, *Mater. Horiz.* 7 (2020) 835-842.
- [171] J.P. Kruth, P. Mercelis, J. Van Vaerenbergh, L. Froyen, M. Rombouts, *Rapid Prototyp. J.* 11 (2005) 26-36.
- [172] M. Vaezi and S. Yang, *Virtual Phys. Prototyp.* 10 (2015) 123-135.
- [173] Y. Tlegenov, W.F. Lu, G.S. Hong, *Prog. Addit. Manuf.* 4 (2019) 211-223.
- [174] I. Pires, B. Gouveia, J. Rodrigues, R. Fonte, *Rapid Prototyp. J.* 20 (2014) 413-421.
- [175] H. Quan, T. Zhang, H. Xu, S. Luo, J. Nie, X. Zhu, *Bioact. Mater.* 5 (2020) 110-115.
- [176] Q. Cheng, Z. Zhang, G. Zhang, P. Gu, L. Cai, *Proc. Inst. Mech. Eng. Pt. C* 229 (2014) 1134-1149.
- [177] M. Hallmann, S. Goetz, B. Schleich, S. Wartzack, *Procedia CIRP* 84 (2019) 271-276.
- [178] M. Šljivic, A. Pavlovic, M. Krašnik, J. Ilić, *IOP Conf. Ser.: Mater. Sci. Eng.* 659 (2019), 012082.
- [179] D. Popescu, A. Zapciu, C. Amza, F. Baci, R. Marinescu, *Polym. Test.* 69 (2018) 157-166.
- [180] T. Kozior and C. Kundera, *Procedia Eng.* 192 (2017) 463-468.
- [181] C. Oztan, R. Karkkainen, M. Fittipaldi, G. Nygren, L. Roberson, M. Lane, E. Celik, *J. Compos. Mater.* 53 (2019) 271-280.
- [182] R.H. Hambali, K.M. Cheong, N. Azizan, *IOP Conf. Ser.: Mater. Sci. Eng.* 210 (2017) 012063.
- [183] N. Jayanth, P. Senthil, C. Prakash, *Virtual Phys. Prototyp.*, 13 (2018) 155-163.
- [184] L.M. Galantucci, F. Lavecchia, G. Percoco, *CIRP Annals*, 59 (2010) 247-250.
- [185] A. Garg, A. Bhattacharya, A. Batish, *Int. J. Adv. Des. Manuf. Technol.* 89 (2017) 2175-2191.
- [186] M. Mehdikhani, L. Gorbatikh, I. Verpoest, S.V. Lomov, *J. Compos. Mater.* 53 (2018) 1579-1669.
- [187] E.A. Papon, A. Haque, S.B. Mulani, *Compos. Pt. B-Eng.* 177 (2019) 107325.

- [188] K.R. Hart, R.M. Dunn, J.M. Sietins, C.M. Hofmeister Mock, M.E. Mackay, E.D. Wetzel, *Polymer* 144 (2018) 192-204.
- [189] S. Singh, M. Singh, C. Prakash, M.K. Gupta, M. Mia, R. Singh, *Int. J. Adv. Manuf. Technol.* 102 (2019) 1521-1536.
- [190] J.-H. Hong, T. Yu, Z. Chen, S.-J. Park, Y.-H. Kim, *Mod. Phys. Lett. B* 33 (2019) 1940025.
- [191] S. Rangisetty and L.D. Peel, in: *Proceedings of the ASME Conference on Smart Materials, Adaptive Structures and Intelligent Systems Snowbird, U. S., September 21-23, 2017.*
- [192] V. Shanmugam, O. Das, K. Babu, U. Marimuthu, A. Veerasimman, D.J. Johnson, R.E. Neisiany, M.S. Hedenqvist, S. Ramakrishna, F. Berto, *Int. J. Fatigue* 143 (2021) 106007.
- [193] M.T.A. Ansari, K.K. Singh, M.S. Azam, *J. Reinf. Plast. Compos.* 37 (2018) 636-654.
- [194] M. Waseem, B. Salah, T. Habib, W. Saleem, M. Abas, R. Khan, U. Ghani, M. Ur, M. Siddiqi, *Polymers* 12 (2020) 2962.
- [195] M. Mohammadzadeh, A. Imeri, I. Fidan, M. Elkelany, *Compos. Pt. B-Eng.* 175 (2019) 107112.
- [196] H. Zhang, D. Yang, Y. Sheng, *Compos. Pt. B-Eng.* 151 (2018) 256-264.
- [197] H. Al Abadi, H.-T. Thai, V. Paton-Cole, V.I. Patel, *Compos. Struct.* 193 (2018) 8-18.
- [198] Z. Hou, X. Tian, Z. Zheng, J. Zhang, L. Zhe, D. Li, A.V. Malakhov, A.N. Polilov, *Compos. Pt. B-Eng.* 189 (2020) 107893.
- [199] J. Naranjo-Lozada, H. Ahuett-Garza, P. Orta-Castañón, W.M.H. Verbeeten, D. Sáiz-González, *Addit. Manuf.* 26 (2019) 227-241.
- [200] W. Zhang, C. Cotton, J. Sun, D. Heider, B. Gu, B. Sun, T.W. Chou, *Compos. Pt. B-Eng.* 137 (2018) 51-59.
- [201] S. Dul, L. Fambri, A. Pegoretti, *Compos. Pt. A-Appl. Sci. Manuf.* 85 (2016) 181-191.
- [202] W. Jing, C. Hui, W. Qiong, L. Hongbo, L. Zhanjun, *Mater. Des.* 116 (2017) 253-260.
- [203] Q. He, H. Wang, K. Fu, L. Ye, *Compos. Sci. Technol.* 191 (2020) 108077.